Final Report
on
SPC 98-4070

COMPUTATIONAL DAMAGE MODEL FOR THERMOVISCOELASTIC LAMINATED COMPOSITES
Phase III

Developing the Breakup Criterion and the Damage Constants in Impact Experiments.

Principle Investigator:
Prof. Dr. Sc. (hab) *N.N. Smirnov*
Investigators:
Prof. Dr. Sc. (hab) *A.B. Kiselev*
M. Sc. *V.F. Nikitin*
Dr. *V.M. Shevtsova*
Dr. *M.V. Yumashev*

Moscow – Brussels – 1999

REPORT DOCUMENTATION PAGE

Form Approved OMB No. 0704-0188

1. AGENCY USE ONLY (Leave blank)	2. REPORT DATE	3. REPORT TYPE AND DATES COVERED
	1999	Final Report

4. TITLE AND SUBTITLE

Computational Damage Model for Thermoviscoelastic Laminated Composites. Third Phase: Model Parameters Development

5. FUNDING NUMBERS

F61775-98-WE083

6. AUTHOR(S)

Prof. Nikolai Smirnov

7. PERFORMING ORGANIZATION NAME(S) AND ADDRESS(ES)

Moscow State University
Faculty of Mechanics and Mathematics
Moscow 119899
Russia

8. PERFORMING ORGANIZATION REPORT NUMBER

N/A

9. SPONSORING/MONITORING AGENCY NAME(S) AND ADDRESS(ES)

EOARD
PSC 802 BOX 14
FPO 09499-0200

10. SPONSORING/MONITORING AGENCY REPORT NUMBER

SPC 98-4070

11. SUPPLEMENTARY NOTES

12a. DISTRIBUTION/AVAILABILITY STATEMENT

Approved for public release; distribution is unlimited.

12b. DISTRIBUTION CODE

A

13. ABSTRACT (Maximum 200 words)

This report results from a contract tasking Moscow State University as follows: The contractor will investigate methods for numerical solution of the inverse problems by developing the constants and comparing theoretical and experimental results, based on the developed theory of thin-shelled damageable composite tubes twisting and axial loading. Further task descriptions are found in the contractor's proposal dated 2 March 1998.

14. SUBJECT TERMS

EOARD, Composites

15. NUMBER OF PAGES

49

16. PRICE CODE

N/A

17. SECURITY CLASSIFICATION OF REPORT	18. SECURITY CLASSIFICATION OF THIS PAGE	19. SECURITY CLASSIFICATION OF ABSTRACT	20. LIMITATION OF ABSTRACT
UNCLASSIFIED	UNCLASSIFIED	UNCLASSIFIED	UL

Final Report
on
SPC 98-4070

COMPUTATIONAL DAMAGE MODEL FOR THERMOVISCOELASTIC LAMINATED COMPOSITES
Phase III

Developing the Breakup Criterion and the Damage Constants in Impact Experiments.

Principle Investigator:
Prof. Dr. Sc. (hab) *N.N. Smirnov*
Investigators:
Prof. Dr. Sc. (hab) *A.B. Kiselev*
M. Sc. *V.F. Nikitin*
Dr. *V.M. Shevtsova*
Dr. *M.V. Yumashev*

Moscow – Brussels – 1999

Contents

Summary

The present paper contains the model description for developing the damage parameters under the conditions of high rates of loading in impact experiments (Chapter 5). The worked out methodology is illustrated on an example of processing the experimental results and spallation of organic materials to develop the critical dissipation energy (Chapter 6). The results of the present investigations show that the dynamical wave pattern generated as a result of impact in the samples depends strongly on the damage parameters. Thus the enthropy growth factors for the shear and tension as well as the breakup criterion – the critical value for the dissipation – could be developed. Those damage parameters for the organic glasses were developed based on an impact experiment.

Chapter 5.
Developing the damage parameters in experiments on impact loading of flat plates.

The experiments on twisting and tension of turbular samples, described in the previous report enable to determine the damage parameters for materials but do not allow to evaluate with a satisfactory accuracy the critical value of dissipation D_*, being the main breakup criterion. The results of numerical investigations show that on approaching the breakup conditions strains and dissipation start growing very rapidly, that does not allow to determine D_* with a necessary accuracy. Thus the experiments on high rates of loading could be used to evaluate the critical damage parameters wherein the multiple waves reflections in the sample and formation of spallation free surfaces make it possible to detect the critical parameters with a greater precision.

The present chapter describes experimental and theoretical aspects of the problem of dynamical deforming and fracture of flat plates in a hypervelocity impact of a thin plate or in dynamical loading by exploding a high explosive charge. As it will be seen, the experimental methodic, allowing to determine the critical damage parameters with a higher accuracy is much more complicated itself as well. The main goal of those experiments is to initiate a strong shock wave in the sample with a sufficiently high amplitude the structural changes (accumulation of damages) to take place. Then tracking the wave and its reflections enables to retrieve the information on the depth of structural changes in the material.

5.1. Experiments on flat plates collisions and loading of plates in explosions.

A simplest method to initiate in a plate a strong shock wave with an amplitude ~10–100 GPa is to perform an explosion of a high explosive on the surface of the plate [1]. The application of explosive lenses guarantees the formation of flat detonation waves loading samples. But it is very difficult to achieve a uniform distribution of parameters behind the wave in a radial direction. The pressure drops down behind the detonation wave very rapidly that makes precise measurements very complicated.

To avoid those difficulties different devices for loading materials were developed based on plate's loading in collision with an impactor-plate moving at a high velocity. Under the present experimental conditions a plane shock wave is initiated in the plate with the parameters behind the wave sustained constant during the time interval necessary for the reflected shock wave to circulate in the impactor-plate. The relatively large transverse length-scales for the sample-plate and the impactor-plate ensure a one-dimensional flow during the time interval necessary to perform measurements. Acceleration of the impactor-plates could be performed in explosions of high explosives or in pneumatic or powder guns.

Fig. 1 illustrates the scheme of the most widely spread device accelerating impactors in a reflected detonation wave (L.V. Altshuller, G.I. Kanel et al., [1]). The device makes it possible to accelerate metallic or plastic impactors 1–10 mm thick up to velocities of 1–6 km/s. The impactor preserves the flat shape despite the fact that the radial expansion of detonation products lowers down the pressure in the peripheral zones much faster than in the center of the impactor. The compensation of the momentum in the peripheral zones of the impactor is achieved by using a focusing ring bringing to an increase of pressure in the peripheral zones due to detonation products in flow into the cavity bounded in the periphery by the focusing ring.

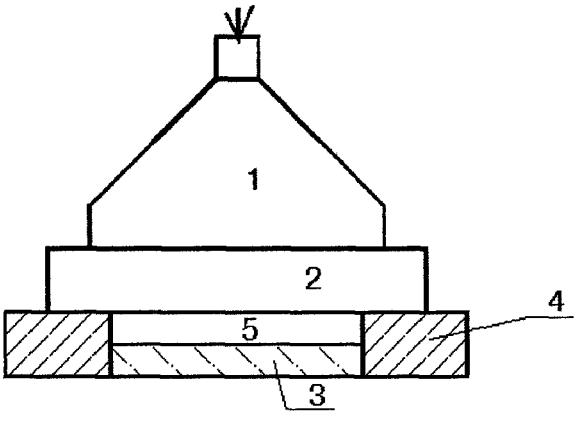

Fig. 1. The scheme of a hypervelocity accelerator of flat impactor-plates
1 – plane detonation wave generating lens; 2 – high explosive charge; 3 – impactor-plate to be accelerated; 4 – steef focusing ring; 5 – air-filled cavity.

In direct acceleration of a plate by expanding detonation products it is difficult to get final velocity less than 1 km/s. To lower down the impactor-plate velocity the damping plates are used (Fig. 2) possessing higher dynamic strength than impactors: $\rho_2 a_2 > \rho_3 a_3$ (ρ – density, a – sonic velocity). The scheme of such a device is given in Fig. 2. The explosive lens 1 generates a flat shock wave in the damping plate 2. Owing to the differences in dynamic strengths of the materials of damping-(2) and impactor-(3) plates the last achieves in reflection of the shock wave from the free surface the velocity higher than that achieved by the damping plate and separates from it in a free flight. The softening polyethylene plate 4 serves to prevent from the impactor plate from spallation. The devices shown in Fig. 2 are attractive as they could be used for acceleration of very thin impactors: foils or films.

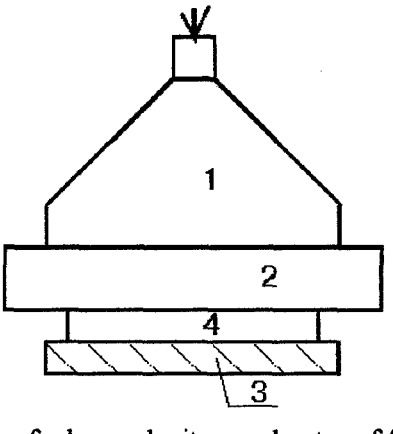

Fig. 2. The scheme of a low-velocity accelerator of flat impactor-plates
1 – explosive lens; 2 – damping plate; 3 – impactor plate to be accelerated; 4 – amortizator.

The explosive lenses (Figs. 1 and 2) are rather convenient accelerators making it possible to control amplitudes and duration of dynamical loadings in a rather wide range. Nevertheless the best controllable conditions for measurements are still provided by pneumatic or powder guns. The more precise impact velocity control and the highest level of uniformity of the zone of one-dimensional deforming could be achieved using the pneumatic accelerators.

To investigate the mechanical properties of shock-waves loading pneumatic 50–150 mm guns are normally used (G.V. Stepanov et al., [1]). The length of the gun up to 14 m and the initial pressure of gas (N_2 or He) in the chamber up to 150 Bar the impact velocities could be varied from 20 m/s up to 1500 m/s. Using the multi-stage light-gas guns could increase the impact velocities up to 8 km/s.

To register the structure of compression waves induced in the sample-plate on colliding the impactor a series of methods was developed for continuous registration of high frequency tensions and velocities variations in the internal sections of the sample and on the contact and free surfaces.

The basic method for registration of tensions in the internal crossections of samples is the method of manganine ganges first applied by P.W. Bridgeman [] for static conditions and then generalized for the dynamic loadings (K.I. Baryshev, G.I. Kanel et al., [1]). The use on manganine ganges is based on the relatively high sensitivity of the material electric conductivity to pressure variations, and relatively low sensitivity of the electric conductivity to temperature variations. To register pressures in plane waves the sensitive element of the gange in the form of an arch 10–30 mm thick covering an area of 0.1–1 sm^2 is used. The gange is placed between the plates forming the sample separated on both sides by thin films (Fig. 3). The electric current through the gange makes it possible to register the power drop variations in the gange caused by pressure variations. To improve the quality of the electric signal normally the induction sources of current are used providing 5–10 A during the time interval of ~100 ms. The gange is connected as one of the components of the resistance bridge or some other differential registration schemes are used to exclude the constant signal determined by the initial resistance of the gange thus increasing the accuracy of measurements.

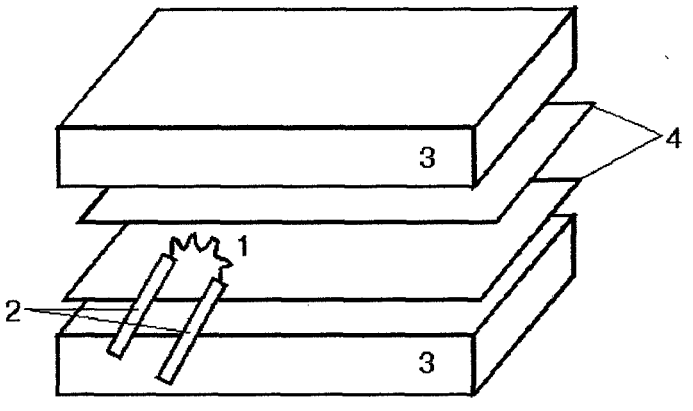

Fig. 3. The scheme of a manganine pressure gange installation in a sample
1 – the sensitive element of a gange; 2 – the contacts of the sensitive elements; 3 – the two pieces of a sample-plate; 4 – isolating films.

The peculiarities of the calibration of the pressure ganges are described in details in [1].

Contrary to pressure measurements the velocity measurements in shock waves are based on the fundamental physical laws and do not need development of any complete calibration diagrams. The methods could be considered the primary ones from the metrological point of view, thus one should a higher precision using these methods.

To perform a continuous registration of the dynamics of a free surface of a metallic sample the method of measures condensator is used (A.I. Ivanov, S.A. Novikov, [1]). An example of the experiment using the measuring condensator to determine the velocity profile of the free surface of the sample is given in Fig. 4. A flat electrode 7 is located at a given distance x_o from the free surface of the sample 5. The electrode and the sample form the measuring condensator (C_m). The electric power is supplied by the source E (big condensator) via resistors R_{in}. The resistance of R_{in} is chosen rather small to provide a small characteristic time $\tau = R_{in} \cdot C_m$ much less than the time of registration. The protective ring 6 is destined to maintain the uniformity of the measuring electrode 7.

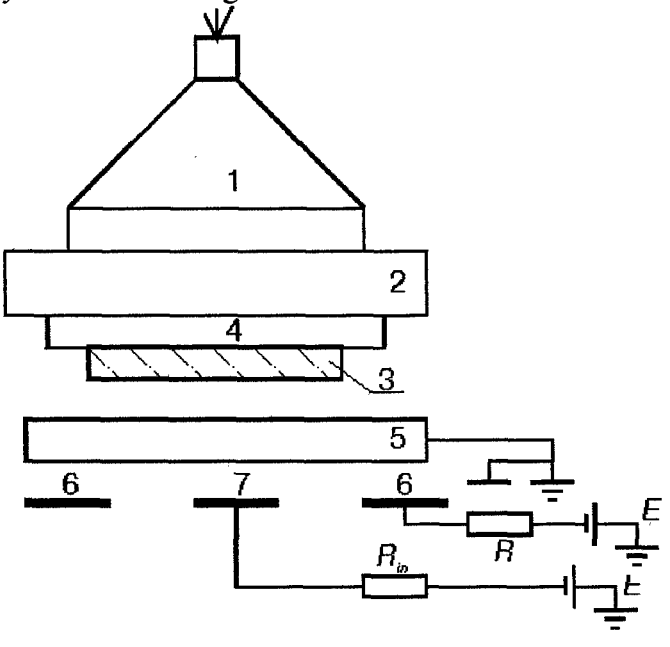

Fig. 4. The scheme of experimental registration of the free surface velocity of a sample-plate in impact loading

1 – the high explosive lens; 2 – damping plate; 3 – the impactor plate; 4 – amortization layer; 5 – the sample-plate (metallic); 6 – the ring; 7 – the measuring electrode; E – the power source; $R = R_{in}$ – resistors.

After the free surface of the sample comes to motion the volume of the measuring condensator begins to decrease inducing a current in the electrical chain. The electrical current is proportional to the velocity of the measuring condensator volume variations, i.e. to the velocity of the sample free surface motion:

$$i(t) = U\frac{dC_m}{dt} = \frac{\varepsilon AU}{4\pi x^2(t)}w(t); \quad w(t) = \frac{dx}{dt} \tag{1.1}$$

where U is the power of the electric source, ε is the dielectrical permeability, A – the area of the measuring electrode, $x(t)$ – the variable distance between the sample-plate and the electrode. The $x(t)$ function could be determined on integrating the equation

$$\frac{dx}{dt} = \frac{4\pi i(t)}{\varepsilon AU}x^2(t); \quad x(0) = x_o \tag{1.2}$$

using the experimentally measured electrical current variations $i(t)$.

The present method is a non-intrusive one. Thus its resolution is limited only by the time shift of the pressure wave coming to the free surface area controlled by the electrode.

To ragister the mass velocities profiles in dielectrical materials the magnetoelectrical method is used (L.V. Altshuller, A.N. Dremin et al., [1]). A Π-shaped gange made of thin aluminum foil is incorporated into the sample for the purpose (Fig. 5). The experimental installation is placed in a uniform constant magnetic field so that the sensitive element of the gange (2) is orthogonal to the magnetic lines and parallel to the shock wave plane. On loading the sample the gange is set into motion with the velocity $v(t)$, and the electric power could be registered on its contacts (3) induced by compression of the magnetic field entrapped by the Π-shaped gange:

$$U(t) = -v(t) \cdot B \cdot l, \tag{1.3}$$

where l is the length of the sensitive element; B – the magnetic induction of the field.

The spatial resolution of the methods for registration of wave profiles by manganine ganges, measuring condensators and magnethoelectric ganges is limited by the characteristic size of the sensitive element of each gange. In the best case the resolution could be several mm in the plane of the shock wave.

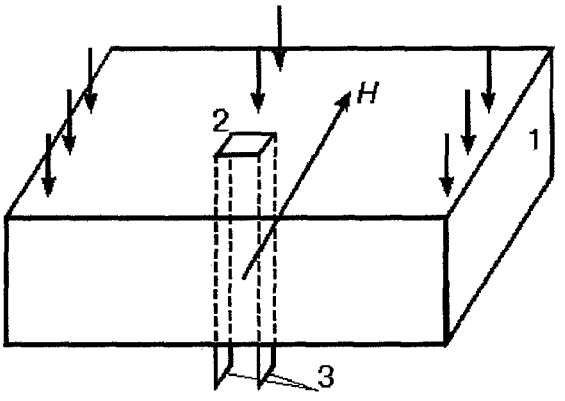

Fig. 5. Registration of a mass velocity variations in the sample using the magnethoelectric method
1 – the sample-plate; 2 – the sensitive foil element; 3 – the conducting contacts of the foil element;
$\vec{H}$ – the magnetic field; short arrows show the direction of the impact compression.

The registration of wave profiles is normally performed by the ray of an oscillograph. Thus the accuracy of registration of current parameters of the material is limited by the accuracy of amplitude measurements of the registration apparatus.

Much higher accuracy of measurements and higher spatial and temporal resolution could be reached using the laser methods for free and contact surfaces motion registration [1].

The lasers application for velocity measurements in experiments with shock waves is based on the Doppler effect. For reflecting free surface velocity ~10–1000 m/s the effect is relatively small (the wave lengths variations is about 10^{-3} – 10^{-2} A). Thus to register the effect two-rays or multi-rays interferometers are used. The measurement then have a differential character that essentially increases the accuracy. The high spatial resolution of the laser methods is due to the fact that the radiation could be focused on a sample in a small spot ~0.1 mm in diameter.

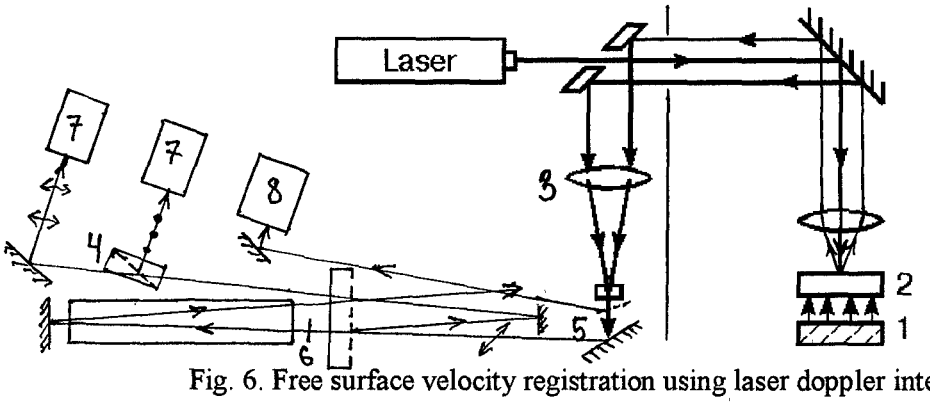

Fig. 6. Free surface velocity registration using laser doppler interferometer
1 – the impactor plate; 2 – the sample plate; 3 – the inlet telescope; 4 – light separator; 5 – polarizer, orientation 45°; 6 – glass lense; 7 – light intensity control registrator; 8 – emitted light registrator.

Fig. 6 shows the scheme of the laser doppler velocity measurements. The application of the method is based on registration of periodical temporal variations of the light intensity in interferention of the two beams of a coherent light with different wave lengths. For the present case the interferention of the light beams reflected from the free surface at different times takes place. For continuously varying velocity of the reflecting surface the Doppler effect for the two beams would be different due to the time shift. The periodical temporal variations of the light intensity registered by the two-rays interferometers have the frequency proportional to the acceleration of the reflecting plate and the relative time shift. A more detailed description of the method could be found in [1].

Thus the modern physics of hypervelocity loadings has a wide spectrum of methods for measurements of kinematic characteristics under high pressure short term loading. Along with the discussed methods the pressure profiles registrations by dielectrical and piesoelectrical ganges are used, as well as photochronography methods of the free surface velocity measurements. Laser diagnostics provides the highest accuracy and resolution of the measurements. Nevertheless, more simple methods of registration are effective as well being applied for some particular problems. For example, measuring condensators provide accurate and easily processible data in experiments on spallation and in experiments aimed at determining the dynamic elasticity limits for metals. Manganine and magnethoelectrical ganges provide the possibility of receiving information from internal layers of samples, that is of importance for many practical issues.

To develop new model parameters for materials using the techniques described above it is necessary to pose and solve theoretically the problem of dynamical behavior of a sample plate under the given loading conditions and by varying the model parameters math the results of dynamical experiments.

5.2. Mathematical statement of the problem.

Regard the problem of hypervelocity deforming and fracture of a flat sample-plate in impact of a flat impactor-plate at a relative velocity V_o. One phase materials will be registered to begin with.

The transverse size of the plates being much larger then the thickness and the characteristic time of the process being relatively small (several reflections of the elastic wave from free surfaces of the sample plate), the problem could be regarded within the flames of one-dimensional approximation (axially deformed state) and adiabatic approximation (div $\vec{q} = 0$; $\vec{q}$ – the heat flux vector). Under the assumptions the mass, momentum and energy equations

take the following form in a coordinate system *(x,y,z)* with *x*-axis orthogonal to free surfaces of plates [2, 3]:

$$\frac{\dot{\rho}}{\rho} = -\dot{\varepsilon}_x, \quad \dot{\varepsilon}_x = \frac{\partial v}{\partial x}; \tag{2.1}$$

$$\rho \dot{v} = \frac{\partial \sigma_x}{\partial x}; \tag{2.2}$$

$$\rho T \dot{\eta} = \frac{(\sigma_x - \sigma_y)^2}{3\mu\tau} + \Lambda \dot{\omega}^2 + A\dot{\alpha}^2; \tag{2.3}$$

where ρ – density of the material; $v = v_x$ – velocity; $\dot{\varepsilon}_x = \dot{\varepsilon}_{xx}$ – the strain rate being the sum of elastic and viscous components: $\dot{\varepsilon}_x = \dot{\varepsilon}_x^e + \dot{\varepsilon}_x^v$; $\sigma_x = \sigma_{xx}$, $\sigma_y = \sigma_{yy} = \sigma_{zz}$ – stress tensor components; T – absolute temperature ($T = T_o$ in the initial state); η – specific entropy (per mass unit); μ – shear modulus; τ – the relaxation time for the viscoelastic media of a Maxwell type; ω, α – damage parameters for the material (for damages in tension ω and damages in shear α) [4].

The temperature T in (2.3) can be determined by the following formula:

$$T = T_o\left(1 - \frac{K\alpha_v}{\rho C_\varepsilon}\varepsilon_x + \frac{\eta}{C_\varepsilon}\right), \tag{2.4}$$

where $K = \lambda + \frac{2}{3}\mu$ – the volume modulus (λ – Lamet coefficient); C_ε – heat capacity of the material under constant deformations; α_v – volume expansion coefficient for the material.

The governing system of state equations for damageable homogeneous thermoviscoelastic media have the following form [4]:

$$\sigma_x = \lambda\varepsilon_x + 2\mu\varepsilon_x^e - \frac{K\alpha_V}{C_\varepsilon}T_o\eta + \Lambda\Omega\ln(1-\omega) + \sqrt{\frac{2}{3}}\frac{AC}{1-\omega}\ln(1-\alpha)\cdot sign\ \varepsilon_x^e;$$

$$\sigma_y = \sigma_z = \lambda\varepsilon_x + 2\mu\varepsilon_y^e - \frac{K\alpha_V}{C_\varepsilon}T_o\eta + 2\Lambda\Omega\ln(1-\omega) - \sqrt{\frac{2}{3}}\frac{AC}{1-\omega}\ln(1-\alpha)\cdot sign\ \varepsilon_x^e;$$

$$\dot{\varepsilon}_x^v = \frac{\sigma_x - \sigma_y}{3\mu\tau}; \quad \dot{\varepsilon}_y^v = \dot{\varepsilon}_z^v = -\frac{\sigma_x - \sigma_y}{6\mu\tau}; \tag{2.5}$$

$$\dot{\varepsilon}_x^e = \dot{\varepsilon}_x - \dot{\varepsilon}_x^v; \quad \dot{\varepsilon}_y^e = \dot{\varepsilon}_z^e = \frac{\sigma_x - \sigma_y}{6\mu\tau};$$

$$\dot{\omega} = \Omega\left(\frac{\varepsilon_x}{1-\omega} - \varepsilon_*\right) H(\varepsilon_x - \varepsilon_*(1-\omega));$$

$$\dot{\alpha} = C\left(\sqrt{\frac{2}{3}}\frac{\left|\varepsilon_x^e - \varepsilon_y^e\right|}{(1-\omega)(1-\alpha)} - \varepsilon_\tau^*\right) H\left(\left|\varepsilon_x^e - \varepsilon_y^e\right| - \sqrt{\frac{3}{2}}(1-\omega)(1-\alpha)\varepsilon_\tau^*\right).$$

Here $\Lambda, \Omega, \varepsilon_*, A, C, \varepsilon_\tau^*$ – material constants related to damage parameters ω and α respectively; $H(x) = \left\{1 \text{ for } x > 0;\ 0 \text{ for } x \le 0\right\}$ – the Heavyside function.

The breakup criterion (the spallation formation criterion for the present case) is that of critical specific dissipation, i.e. the specific dissipation of material should not exceed the critical value D_* [2, 3[:

$$\int_0^{t_*} \frac{1}{\rho}\left(\frac{(\sigma_x - \sigma_y)^2}{3\mu\tau} + \Lambda\dot{\omega}^2 + A\dot{\alpha}^2\right) dt \le D_*. \qquad (2.6)$$

Here t_* – the breakup time, D_* – the damage constant of critical dissipation.

Initial conditions are the following:

a) for the impactor-plate

$$v = V_o,\ \rho = \rho_{o1},\ \sigma_x = 0,\ T = T_o,\ \eta = 0,\ \alpha = \omega = 0,\ (-h \le \overset{o}{x} \le 0);$$

b) for the sample-plate

$$v = 0,\ \rho = \rho_{o2},\ \sigma_x = 0,\ T = T_o,\ \eta = 0,\ \alpha = \omega = 0,\ (0 \le \overset{o}{x} \le H),$$

where $\overset{o}{x} = x\big|_{t=0}$ – lagrangian coordinate; h, H – thicknesses of the impactor and the target respectively (Fig. 7).

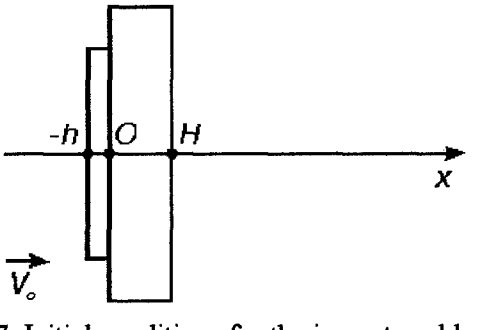

Fig. 7. Initial conditions for the impact problem

The boundary conditions on the contact surface $\overset{o}{x} = 0$ are the following:

a) for the case of compression ($\sigma_x < 0$)

$$v^+ = v^-,\quad \sigma_x^+ = \sigma^-;$$

b) for the opposite case a free surface condition should be used

$$\sigma_x = 0.$$

The boundary conditions on the spallation breakup surfaces that could be formed in different crossections of the target are similar to free surface conditions. The spallation surfaces should be introduced into the solution in the crossections where the breakup criterion (4.6) was satisfied.

The boundary conditions on free surfaces $\overset{o}{x} = -h$ and $\overset{o}{x} = H$ are:

$$\sigma_x = 0.$$

Now regard the problem of deforming and spallation breakup of a plate in its loading by the detonation products of a high explosive layer h_E thick put in contact with the plate.

The equations (2.1) – (2.5) describe the dynamical processes inside the plate. The equation (2.6) gives the breakup criterion. The boundary condition for the free surface $\overset{o}{x} = H$ is similar to that for impact loading:

$$\sigma_x = 0.$$

The boundary condition on the surface contacting the high explosive has the following form:

$$\sigma_x\big|_{\overset{o}{x}=0} = -P(t),$$

where $P(t)$ is the pressure of the detonation products at the interface.

It is assumed that the outset of the plane detonation wave takes place at $\overset{o}{x} = -h_E$, and by the time $t = 0$ the detonation wave approaches the front surface of the plate ($\overset{o}{x} = 0$), and the plate at $t = 0$ is not deformed and/or stressed.

Assuming that the equation of state for the detonation products is

$$p = G\rho^3,$$

and neglecting the transverse expansion of the products one can obtain an exact formula for the pressure variation on a moving front interface of the plate [5]:

$$P(t) = \frac{16}{27}\rho_E U_D^2 \left(\frac{1 + \dfrac{w}{h_E}}{1 + \dfrac{U_D t}{h_E}} - \frac{1}{U_D}\frac{dw}{dt} \right)^3, \qquad (2.7)$$

where U_D is the velocity of the detonation wave, ρ_E – the density of the charge, w – the displacement of the front surface of the plate ($\overset{o}{x} = 0$).

5.3. A short note on the numerical solution.

The described above problems were solved numerically in lagrangian coordinate system deforming and moving with the media. The explicit finite-difference scheme of the second order of accuracy of the Wilkins type was used [6, 7]. The eulerian coordinates x_i and

velocities v_i were determined in the grid nodes $\overset{o}{x}_i$. The other parameters: strain rates $(\dot{\varepsilon}_x)_{i+1/2}$, deformations $(\varepsilon_x)_{i+1/2}$, densities $\rho_{i+1/2}$, masses of cells $\varphi_{i+1/2} = \rho_{i+1/2}(x_{i+1} - x_i)$, stresses $(\sigma_x)_{i+1/2}$, etc. – were determined in the centers of cells.

To guarantee the stability of the calculations the time step was chosen based on the Courant criterion

$$\Delta t = \frac{0.25}{\max\left\{\dfrac{a_{i-1/2} + |v_i| + |v_{i-1}|}{\overset{o}{x}_i - \overset{o}{x}_{i-1}}\right\}}.$$

The negative stresses on the contact surfaces were determined using the condition of the equality of velocities. For all the other cases the velocities on both sides of the contact surface were determined using the condition $\sigma_x = 0$.

A special mechanism to distinguish the surfaces of spallation breakup was developed. In case the dissipation D determined by formula (2.6) surpassed the critical value ($D > D_*$), a spallation surface was assumed to have been formed within the cell $\overset{o}{x}_i < \overset{o}{x} < \overset{o}{x}_{i+1}$. Then the grid was rearranged in the vicinity of the spallation surface so that the nearest nodes were placed to the surface from the both sides to form a contact surface. The following formulas were used to recalculate the parameters

$$\bar{x}_i = \bar{x}_{i+1} = \frac{1}{2}(\overset{o}{x}_i + \overset{o}{x}_{i+1}); \quad \bar{v}_i = \bar{v}_{i+1} = \frac{1}{2}(v_i + v_{i+1}).$$

Thus a new cell of a zero mass was formed:

$$(\bar{\sigma}_x)_{i+1/2} = \bar{\rho}_{i+1/2} = \bar{D}_{i+1/2} = \bar{T}_{i+1/2} = \bar{\eta}_{i+1/2} = 0.$$

The mass of the neighboring cells increased:

$$\bar{\varphi}_{i-1/2} = \varphi_{i-1/2} + \frac{1}{2}\varphi_{i+1/2}; \quad \bar{\varphi}_{i+3/2} = \varphi_{i+3/2} + \frac{1}{2}\varphi_{i+1/2};$$

$$\Delta\varphi_{i-1/2} = \bar{\varphi}_{i-1/2} - \varphi_{i-1/2}; \quad \Delta\varphi_{i+3/2} = \bar{\varphi}_{i+3/2} - \varphi_{i+3/2}.$$

The other parameters of the neighboring cells were determined by formulas:

$$\bar{\rho}_{i-1/2} = \frac{\bar{\varphi}_{i-1/2}}{(\bar{x}_i - \bar{x}_{i-1})}; \quad \bar{\rho}_{i+3/2} = \frac{\bar{\varphi}_{i+3/2}}{(\bar{x}_{i+2} - \bar{x}_{i+1})};$$

$$\bar{f}_{i-1/2} = \frac{(f_{i-1/2}\varphi_{i-1/2} + f_{i+1/2}\Delta\varphi_{i-1/2})}{\bar{\varphi}_{i-1/2}}; \quad \bar{f}_{i+3/2} = \frac{(f_{i+3/2}\varphi_{i+3/2} + f_{i+1/2}\Delta\varphi_{i+3/2})}{\bar{\varphi}_{i+3/2}};$$

$$f = f(\eta, \alpha, \omega, D, T, \varepsilon, \varepsilon^e, \varepsilon^v).$$

The elastic energy in the neighboring cells decreases being spent for the breach formation.

Numerical solution of the problem of the impact loading and spallation formation makes it possible to determine theoretically velocity variation of the free surface of the sample plate, depending on values of the material constants. Comparison of the obtained theoretical curves with experimental results will enable to develop the model parameters. The time and place of spallation formation can be easily detected from experiments thus providing sufficient data to develop the critical dissipation parameter D_*. Some other material constants could be easily developed or verified in dynamic experiments as well. The next chapter will give an example of developing the damage parameters for organic materials and comparing the results with the impact experiment.

References to chapter 5

1. Kanel G.I., Razorenov S.V., Utkin A.V., Fortov V.E. Shock-wave phenomena in condensed media. //Moscow, Yanus-K Pbl., 1996, 408 p.
2. Kiselev A.B., Yumashev M.V. On criteria for dynamical destruction of thermoelastoplastic media. //Moscow Univ. Mechanics Bulletin, Allerton Press, 1990, No 4, pp. 38-44.
3. Kiselev A.B., Yumashev M.V. Deforming and fracture in shock loading. A model for damageable thermoelastoplastic media. //J. Appl. Mech. Techn. Phys., 1990, No 5, pp. 116-123.
4. Smirnov N.N., Kiselev A.B., Nikitin V.F., Shevtsova V.M., Yumashev M.V. First interim report on SPC-97-4046, Moscow-Brussels, 1997, 38 p.
5. Gendugov V.M., Kiselev A.B. Numerical investigation of spallation in a plate loaded by explosion. //Moscow Univ. Mechanics Bulletin, Allerton Press, 1990, No 5, pp. 54-58.
6. Wilkins M.L. Modeling the behavior of materials. //Struct. Impact and Crushworth. Proc. Int. Conf. V.2, L., N-Y.: 1984, pp. 243-277.
7. Kiselev A.B., Rybakin B.P. Numerical investigation of spallation breakup in explosive and impact loading. Bulletin of the Institute for Mathematics of Moldova, Kisheneu, 1989, 39 p.

Chapter 6

Estimation of the damage parameters based on an experiment

This chapter describes an estimation of damage parameters (shear and volumetric kinetic and enthropy factors, [1-5]) based on an experiment of high-velocity flat collision of samples made of plexiglass. The output of the experiment is the velocity of the opposite side of the target per time. The projectile's length is less than the target's; both samples are made of the same material. The width of the samples is much larger than their length so the interaction of the samples is assumed to be flat.

The background of the experiment [6] used in our estimation is the following. The collision process is being developed in microseconds; it begins with the contact of a projectile moving at a high velocity V_0 with a stalling target. A compressive wave is originated; it propagates in both directions producing deformations higher than the elasticity limit. When the wave reaches the opposite side of the target, it starts to move in the direction of the initial velocity V_0. Then the stretching wave originated on the open side of the projectile reaches the open side of the target and the velocity decreases. If this wave has a high amplitude, its reflection from the open side of the target will bring to the beginning of the destruction growth nearby. This process finally brings to separation of a "plate" from the open side of the target. In case of the same materials both of the projectile and the target the size of the plate is close to the size of the projectile. The plate separated moves with the velocity less than initial V_0 in the direction of the projectile before collision. The velocity of the oposite end of the target as well as the velocity of the plate separated is recorded with rather high frequency and accuracy in time.

To estimate the damage parameters we make the following job. We build the mathematical and numerical model for 1D motion of visco-elastic samples which is extended to account the influence of the damages accumulation. This model is described in our previous reports; we have only two types of damage parameters here because the material is uniform. The elastic parameters of the materials, sizes of the samples and the collision velocity V_0 are assumed to be known a priori. Varying the damage parameters (essentially the enthropy and kinetic factors) and processing the numerical calculations we observed that one of the main parameters gained both from the experimental output and the nu-

merical calculations – the maximal velocity of the target's opposite end V_m – depends essentially on a complex combined of the enthropy and the kinetic factors for the shear damage (A and C in our notation). In the conditions of the experiment when the critical deformations are exceeded almost everywhere in the collision process and the duration of the process is several orders less than the relaxation time, the value of V_m is practically independend of other parameters including the enthropy and the kinetic factors for the volumetric damage (Λ and Ω in our notation, correspondingly). The first stage of the work was to obtain the value of this complex.

The other damage parameters, mainly the kinetic and enthropy factors of the volumetric damage, regulate another significant parameter obtained both in the experiments and the calculations – final velocity of the plate separated. The shape of the velocity per time curve before separation is regulated with kinetic factors of both shear and volumetric damage parameters. So all the most difficult to measure damage parameters – the kinetic and enthropy factors – could be estimated with such an experiment.

The value of critical dissipation D_* regulates the time of the breakup and spallation formation, detected on the diagrams, and the final velocity V_f. Thus the value of the critical dissipation D_* for the material could be developed based on the experimentally measured values of the breakup time and final velocity of the spallation plate.

6.1 The parameters used in calculations and in the experiment

The known parameters of the experimental setup [6] sufficient for our investigations are enlisted in the Table 6.1. All the dimensional units are presented in the SI system of measurements.

Parameter	Magnitude	Unit	Description
Kinematic setup parameters			
H	11.7	mm	Length of the target
h	1.4	mm	Length of the projectile
V_0	800	m/s	Velocity of collision
Material (plexiglass) properties			
ρ_0	1180	kg/m^3	Density
μ	1.33	GPa	Shear elastic module
K	6.08	GPa	Volumetric elastic module
α_v	$2.2{\cdot}10^{-4}$	K^{-1}	Thermic expansion factor
C_ε	1350	J/(kg·K)	Specific heat capacity
τ	1000	s	Relaxation time

Table 6.1. Parameters of the experimental setup.

Some remarks must be put for the contents of the Table 6.1. First, the width of the samples (both the projectile and the target) was about 70 mm; it is much higher than

the length of each part of the system so its value is essential to choose 1D model of the process but is not used once the 1D model is chosen. The second remark is about the relaxation time τ. Its physical meaning is the duration of the period when the stresses in a visco-elastic material being strained decrease in $e \approx 2.87$ times. If one can imagine a solid body, the stresses in it release within a significant period of time even the body is very soft. But the whole process of collision takes micro-seconds. If the relaxation time value affects the process of collision it must be also of the order of micro-seconds. It means that the effective dynamic viscosity of such a material must be $\eta = \mu\tau \sim 10^3$Pa·s – this can not be a solid body but a viscous liquid. So we choose a magnitude of the relaxation time several orders higher than this value, and then it can not affect a short-term process at all independently of its actual value. This consideration helps us to eliminate the influence of the relaxation time (which actual value is not known from the experiments) on the collision effects.

The critical deformations ε_* and ε_τ^* which regulate the process of volumetric and shear damages accumulation correspondingly can be estimated roughly to be equal to:

Parameter	Magnitude	Description
Estimates of critical deformations		
ε_*	0.03	Critical volumetric deformation
ε_τ^*	0.015	Critical shear deformation

Table 6.2. Estimates of the critical deformations.

Even the magnitudes of ε_* and ε_τ^* affect the damage accumulation process sufficiently but within the conditions of the experiment when a high-velocity interaction of the samples takes place both estimates of the critical values of deformation are exceeed. They are exceeded considerably (several times) in the compression and decompression waves passing along the samples. Therefore their actual values are of little influence on the process; one thing is very essential only – that the volumetric damages are accumulated only in the stretched but not in the compressed state of the material and the shear stresses are accumulated every time when the corresponding deformation exceeds the limit.

The set of completely unknown damage parameters looks like follows:

Parameter	Unit	Description
Unknown damage parameters to be estimated		
Ω	s^{-1}	Volumetric damage kinetic factor
Λ	Pa·s	Volumetric damage enthropy factor
C	s^{-1}	Shear damage kinetic factor
A	Pa·s	Shear damage enthropy factor
D_*	J/kg	Critical specific dissipation energy

Table 6.3. List of unknown damage parameters.

One of the main goals of the present investigation is to obtain the estimates of the parameters enlisted in the Table 6.3 on the base of the experimental data published in [6].

6.2 Calculations of the collision process: dynamics of parameters

The first set of calculations is made to present the dynamics of the parameters in the process of two samples collision when all the damage parameters accumulation is ignored (the kinetic factors are set to be zero). Really we obtain almost elastic behavior because the relaxation time is much higher than the durarion of the process. The second set compared to the first one is calculated with non-zero damage parameters. All the parameters values except for those enlisted in the Table 6.3 are taken from the Tabs. 6.1-6.2. The process is traced either until a plate separates from the target due to damage or until the decompression wave passes half-way from the opposite (to the collision) side of the target in the direction oriented to the projectile.

6.2.1 The visco-elastic behavior

The figures Fig. 6.1-4 show the development of velocity, deformation, stress and temperature growth versus lagrangian coordinate X for the time moments:

$$t = 0.36(a), 1.02(b), 3.31(c), 5.50(d), 6.38(e), 8.06(f)\mu s.$$

Each moment is chosen to describe different stages of the process; curves relating to each one are denoted with underlined letters from a to f as it is shown above. The direction of waves propagation is denoted with arrows.

The Fig. 6.1 shows the development of velocity. At $t = 0.36\mu$s (curve a) the collision of the projectile (moving at V_0=800m/s) and the target (0m/s) brings to origination of two waves, propagating to the left (into the projectile) and to the right (into the target). The resulting velocity between two waves is two times less than V_0. At $t = 1.02\mu$s (curve b) the wave which was moving to the left has already reflected from the edge of the projectile and propagates to the right behind the leading wave propagating in the target. The velocity changes from $V_0/2$=400m/s to 0m/s in the rear wave. The whole complex then consists of two waves (compression then decompression, see below); the distance between them is approximately the doubled projectile size (since the material is the same). At $t = 3.31\mu$s (curve c) the complex of two waves propagates within the target towards its right edge. At $t = 5.50\mu$s (curve d) the leading wave is reflected from the edge of the target; the velocity on the right edge rises up to V_0=800m/s. At $t = 6.38\mu$s (curve e) the second (rear) wave reflects from the edge; the velocity on the open edge begins to fall down. The leading wave is propagating to the left within the target. At $t = 8.06\mu$s the complex of the leading and the rear waves is propagating within the target to its left edge; the velocity between the waves rises to $V_0/2$=400m/s and then falls to zero.

The Fig. 6.2 shows the stress component σ_{xx} distribution evolution in time. The character of waves is clearly seen from this figure. The initial impact generates two compressive waves (curve a, $t = 0.36\mu$s) – they are loading the samples up to 1.1GPa. The negative value of σ_{xx} indicates the compressive state of material between the waves. After the wave

propagating towards the edge of the projectile reflects, it changes to be a decompression wave (curve b, $t = 1.02\mu s$) but the material of the projectile is never decompressed to the stretched state during this stage of the process; the stresses magnitude drops to zero behind the rear (reflected) wave. The curve c (time moment $t = 3.31\mu s$) shows the wave complex (compression plus decompression) propagating towards the right edge of the target. At the time moment $t = 5.50\mu s$ the leading wave has already reflected from the edge of the target opposite to the impact site; it has changed its character to decompression state and is on its way to collide with the rear wave (which is also decompressive). The collision takes place in the point inside the target; the distance from this point to the right edge of the target equals to the size of the projectile. The result of collision is shown on the curve e (time $t = 6.38\mu s$): the compressed state of the material changed to the stretched state (loading up to 1.1GPa); the leading wave decompresses the material; the rear wave compresses it back. At $t = 8.06\mu s$ the complex of the leading (decompressive) and the rear (compressive) wave is propagating within the target towards the initial impact site. The stress σ_{xx} first rises up to 1.1GPa (positive value means stretching loading), then drops to zero in the rear compressive wave.

The Fig. 6.3 traces the deformation ε_{xx} distribution along the lagrangian coordinate X for the same time moments. It is clearly seen that the behavior of deformation copies the behavior of the stress (Fig. 6.2); this is an expected behavior because the material is practically elastic in this set of calculations and the deformation is proportional to the stress. The maximal deformation module is about 0.17 – this is a very high value exceeding the estimations of the critical deformations ε_* and ε_τ^* several times.

The Fig. 6.4 shows the temperature growth $T - T_0$ in the material of the target and the projectile. As it is expected from nearly elastic behavior, the temperature traces the stress and the deformation, but the sign of the temperature growth is opposite to the sign of the stress σ_{xx}. The maximal temperature change is about 40 degrees Kelvin (total amplitude 80K).

The Fig. 6.5 shows the velocity $V_e(t)$ of the target edge opposite to the impact site per time. It is seen from this figure that the first $\approx 5\mu s$ the velocity is equal to zero (the waves generated by the impact have not reached the edge). Then the velocity rises up to $V_m = V_0$=800m/s and remains high until the rear wave reflects from the edge of the target at $t \approx 6.5\mu s$. Then it falls down to zero.

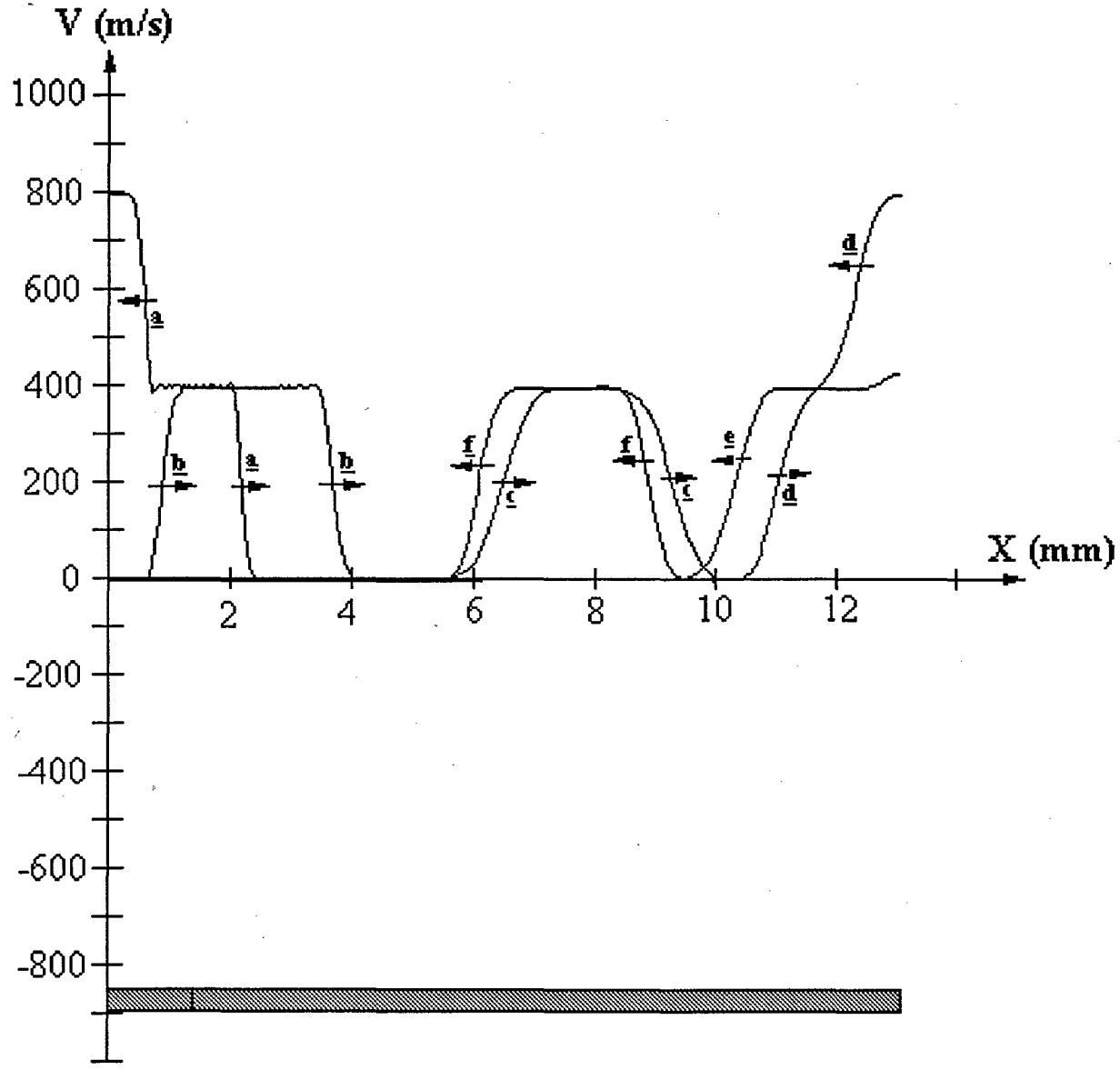
V (m/s)
1000
800
600
400
200
0
-200
-400
-600
-800
2
4
6
8
10
12
X (mm)
a
b
a
b
f
c
f
c
e
d
d

Fig. 6.1.

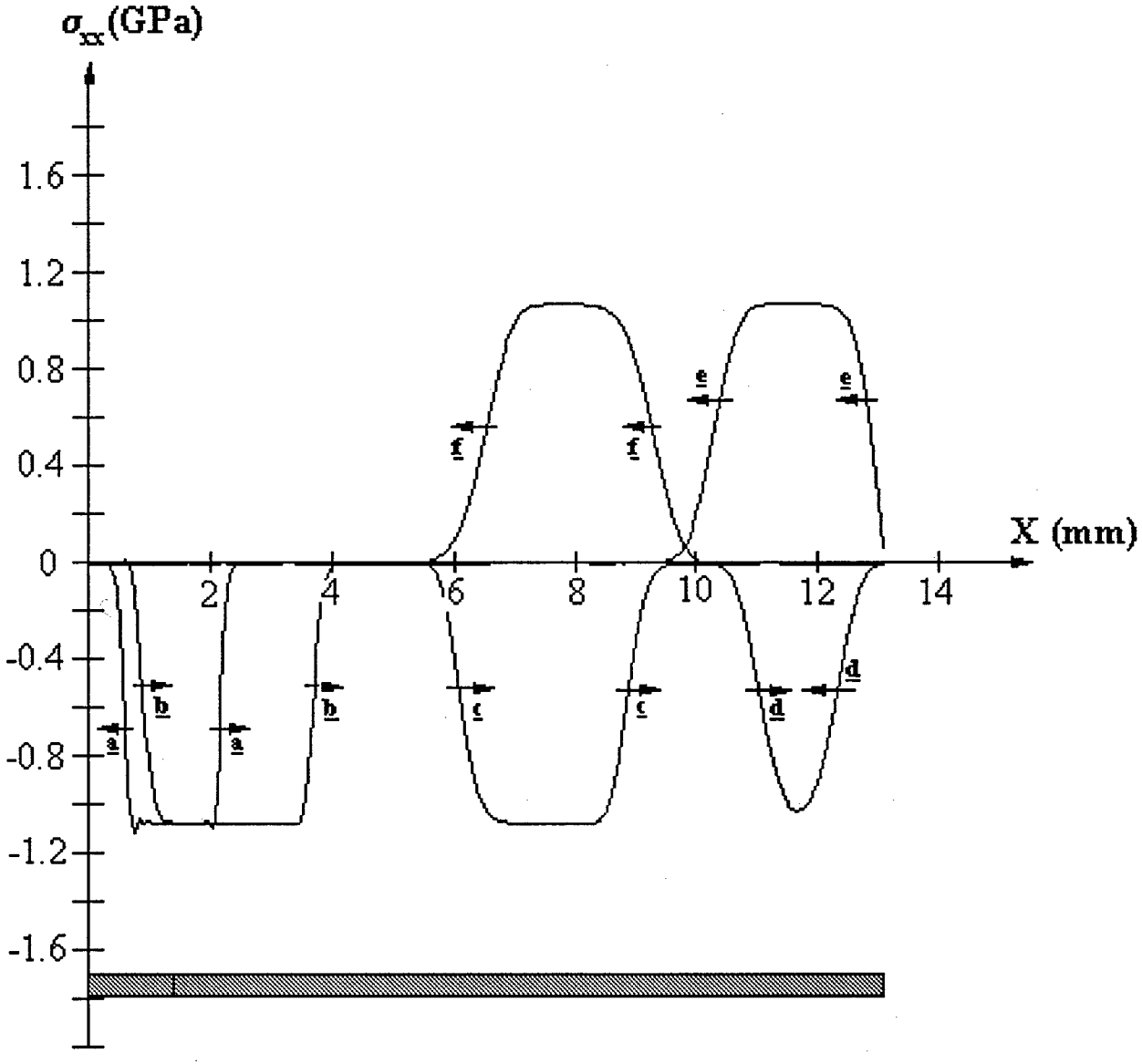

Fig. 6.2.

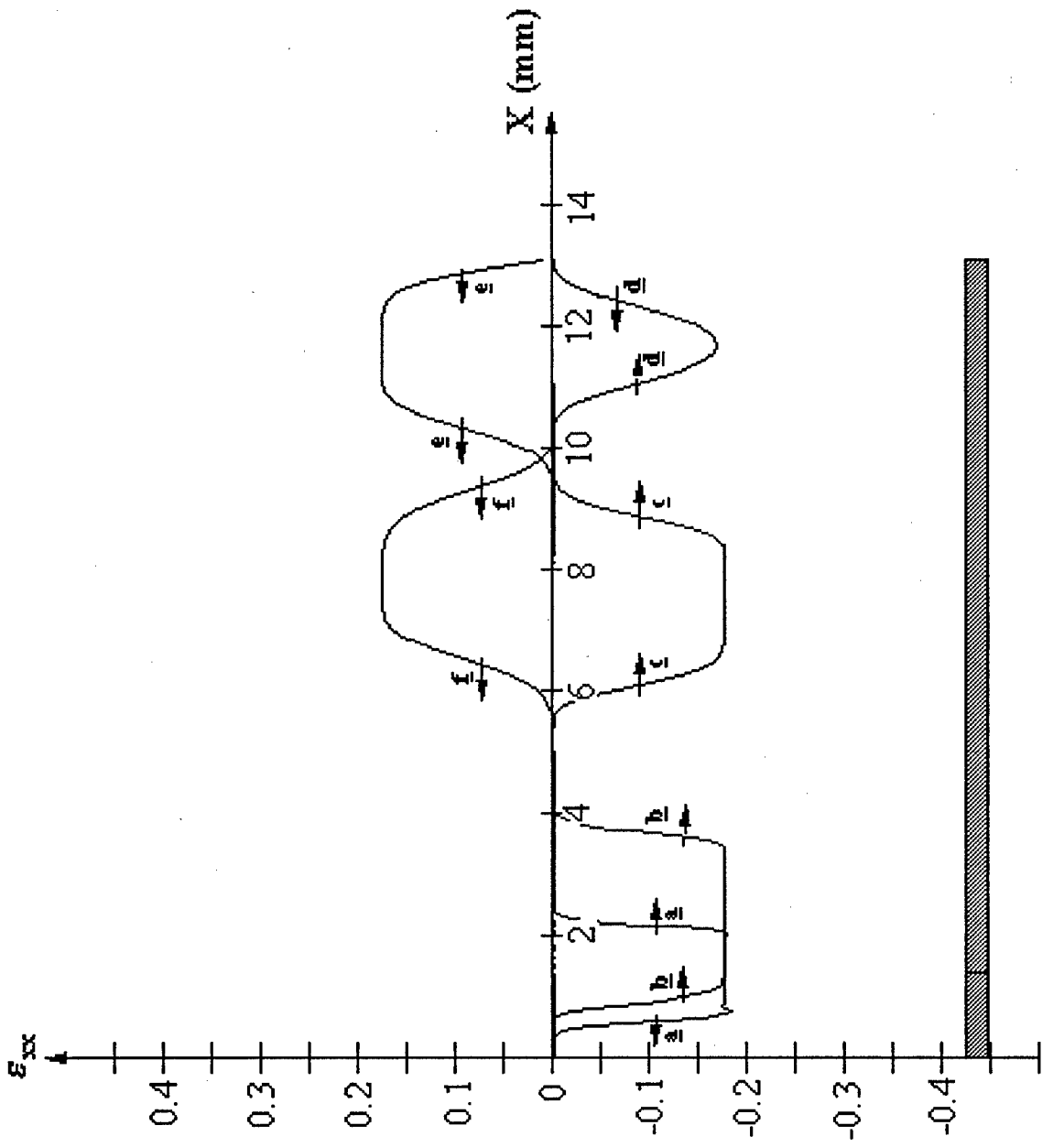

Fig. 6.3.

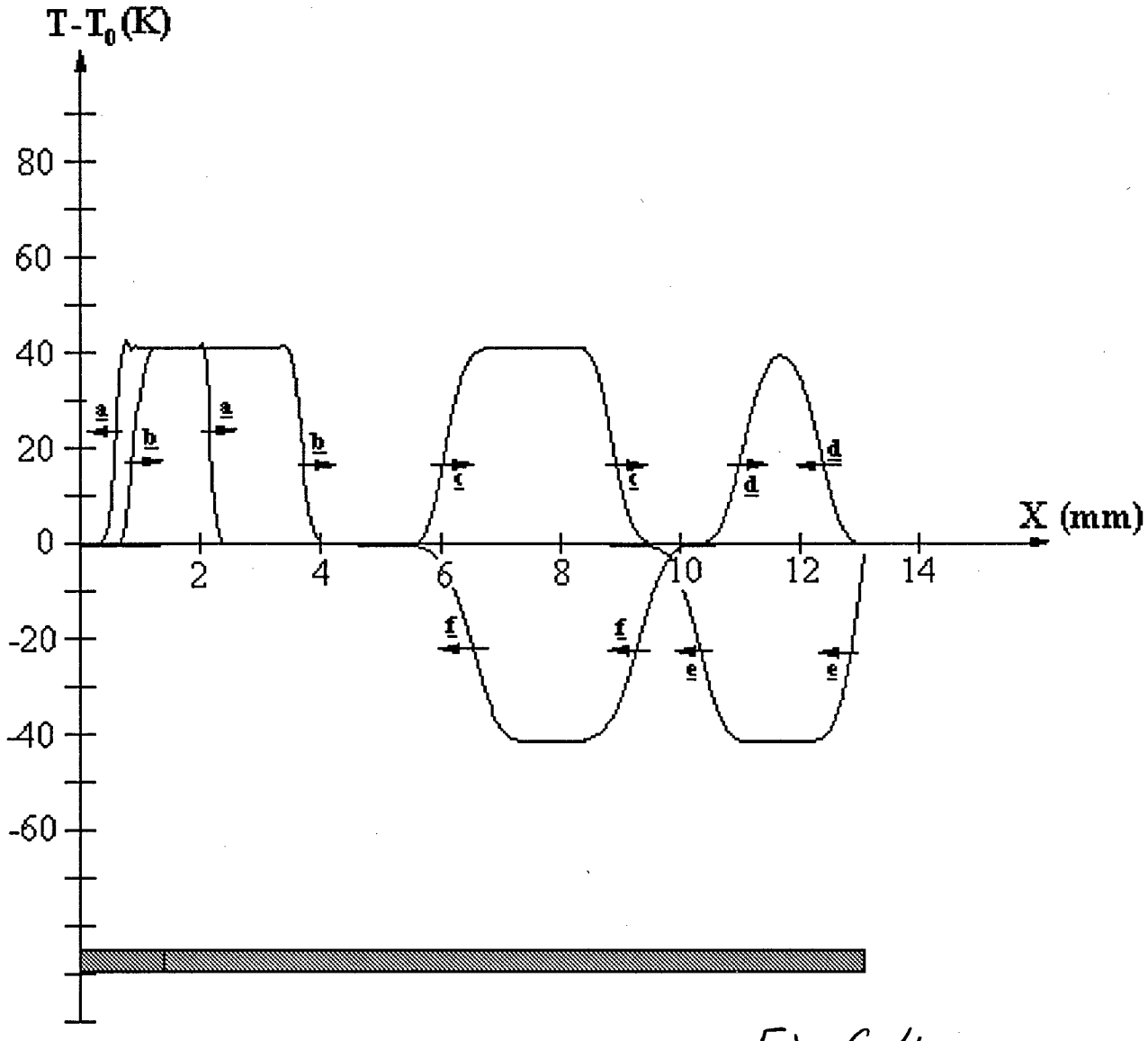

Fig. 6.4.

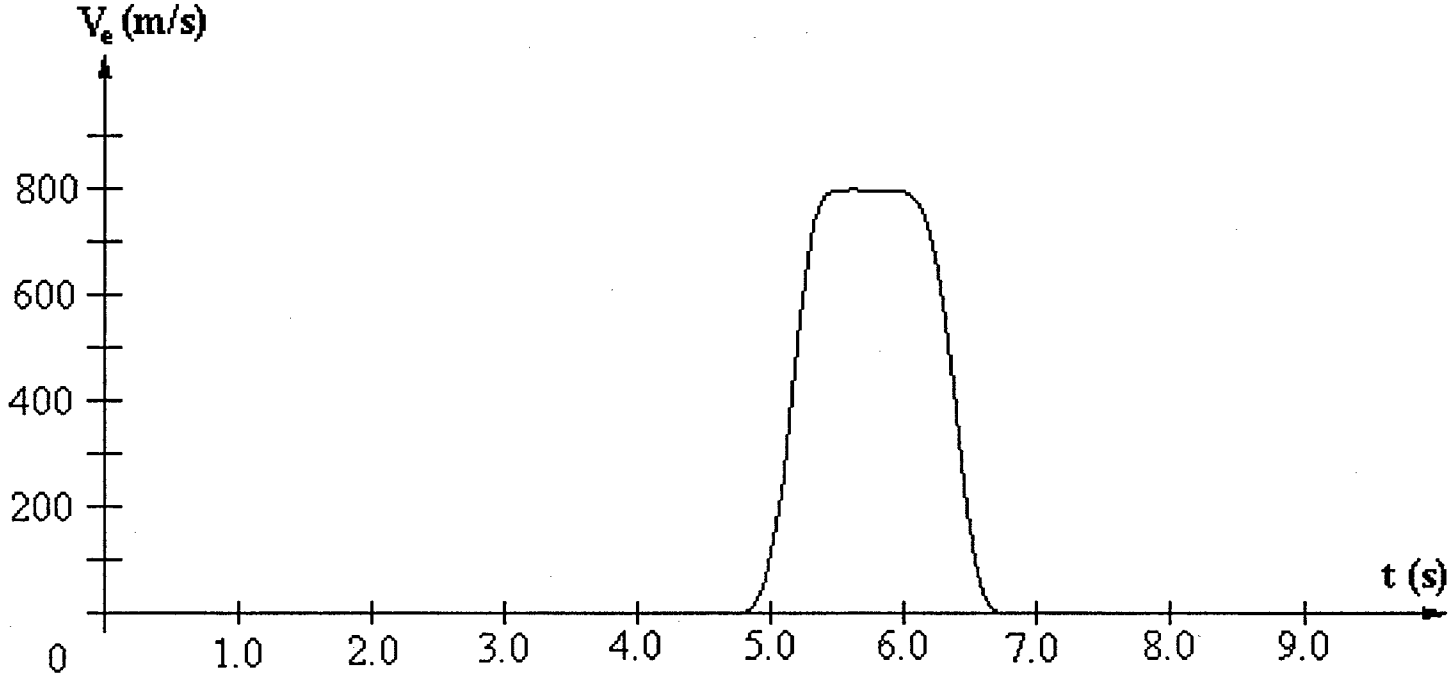

Fig. 6.5.

6.2.2 The behavior of damageable material

To investigate the difference between damageable and visco-elastic behavior of the plexiglass material, the set of calculation analoguous to the previous set for the visco-elastic case was processed. The values of damage parameters enlisted in the Table 6.3 were the following:

$$\Omega = 5 \cdot 10^3, \quad C = 5 \cdot 10^3, \quad \Lambda = 10^7, \quad A = 10^7, \quad D_* = 10^6.$$

All the units of measurement for the parameters above are taken from the Table 6.3. The value of the critical specific dissipation D_* is taken rather high in order to avoid premature breakup taking into account that this set of calculations is processed just to illustrate the new features in the materials behavior arising with the introduction of the damages accumulation model.

The results of calculations are shown in the figures 6.6-13; different curves on the figures 6.6-12 correspond to the following time moments:

$$t = 0.33(a), 1.44(b), 4.07(c), 5.48(d), 6.37(e), 8.23(f)\mu s.$$

The Fig. 6.6 illustrates the development of velocity. The similar wave picture remains for the damageable case, especially at the beginning (curve a, $t = 0.33\mu s$), but then it can be seen (curve b, $t = 1.44\mu s$) that after reflection from the projectile edge the velocity behind the rear wave of the complex does not fall to zero. It is small but positive (aligned with the initial velocity of the projectile) due to dissipation. The velocity behind the leading compressive wave grows less than in the visco-elastic case. The curve c ($t = 4.07\mu s$) shows the wave complex moving within the target to its edge opposite to the impact site; one can see that the plateau between the compressive and decompressive waves is not so high as in the visco-elastic case; it gradually decreases while the wave complex propagates. The curve d ($t = 5.48\mu s$) shows the distribution of velocity when the leading wave has already reflected from the edge of the target; the velocity on this edge is less than V_0 and equals to $\approx$600m/s. When moving backwards, the leading wave (now decompressive) splits into a leading foreshock (with not a very high amplitude) and a decompressive shock (curves e and f) moving at a lower speed. That shock is similar to a Rakhmatulin decompressive shock but for damageable materials. The compressive wave following decompression does not bring the velocity to zero but to the velocity of about 100m/s directed aligned with the initial impact.

The Fig. 6.7 shows the distribution of stress σ_{xx}. After the initial shock the compression rises up to 1.1GPa as in the visco-elastic case (curve a), but then the plateau between the compressive (leading) and the decompressive (rear) waves starts to decrease gradually (curves b and c). For example, the curve c shows that after the initial compression the magnitude of stress rises to $\approx$0.8GPa ($t = 4.07\mu s$) and then it falls back to zero in the rear (decompressive) wave. After the wave complex reflects from the edge of the target (curves d,e) it consists of three waves; the wave pattern originated after the reflection is clearly seen on the curve f, $t = 8.23\mu s$ when it propagates deeply within the target. The first decompressive foreshock is not big; it propagates with the velocity of the elastic wave. The magnitude of decompression after the foreshock is about $\approx$0.06GPa. Then a

strong decompressive shock increases the stress magnitude up to 0.5GPa (this magnitude gradually decreases in time). Then passes the rear (compressive) wave, but now it change the stress not to zero but to a slightly compressed state (-0.03GPa). One can see that the wave development differ essentially from the visco-elastic case (Fig. 6.2), especially after the wave complex reflects from the edge of the target.

The Fig. 6.8 illustrates the development of longitudinal deformation ε_{xx}. The development of deformation differs in this case both from the development of deformation in the visco-elastic case (Fig. 6.3) and from the development of stress (Fig. 6.7) in the damageable case. The two compressive waves originated from the primary impact increase the deformation up to 0.18 (compressed state). After the left wave reflects from the edge of the projectile the wave complex originates and begins to propagate towards the right edge of the target: the leading wave compresses the material to -0.15÷-0.18, then not a plateau but slight continuation of the deformation increase takes place (up to -0.16÷-0.18, see curves b and c), then the decompression wave decreases the compressed state to ≈-0.03, not to zero. The wave complex reflects from the right edge of the target (between time moments for the curves d and e), and the following picture is being observed on the diagrams for the backward motion of the wave complex. The foreshock decreases the primary compressed state a little (the state remains compressed), then the strong shock decompresses the material up to 0.11 deformation, then the decompression rises slightly up to 0.12, then the compression wave decreases the decompressed state to ≈0.05, but then the decompression rises again up to 0.06. In the vicinity of the edge of the target the decompression decreases to zero.

The Fig. 6.9 illustrates the development of temperature. The compressive waves originated after the initial impact increase the temperature by +41 degrees Kelvin, but there is not a plateau between the waves but further increasing of temperature due to dissipation (curve a). The temperature maximum is at the impact site (+44K), and it continues to rise until the wave propagating towards the edge of the projectile reflects from it and passes by the site of impact (curve b). When the wave complex propagates towards the edge of the target (curves b,c) the leading compression brings to the increase of temperature up to ≈40K, then the temperature increases gradually to ≈57K (curve b) ÷ ≈42K (curve c), and then it drops back to about +20K. The decompression of the material arising after the wave complex reflects from the edge of the target brings to decrease of the temperature below the initial state (curves e,f) up to -20K, but it is seen from the curve f that the final state of the temperature on this stage of the process is still positive (about +7K). It can be explained by the energy dissipation in the damageable material.

The development of the damage parameter α which is responsible for the shear damage is shown on the Fig. 6.10. One can see that it begins to rise immideately after the impact and it's maximum remains at the impact site rising rapidly at first (curves a,b) and then slowly (curves c-f). The wave complex propagating towards the edge of the target (curves b,c) brings to rise of the α damage behind the leading wave; the rate of the increase is not as high as of the stress, deformation or temperature because the damage parameter is governed by an equation of the kinetic type with characteristic time much slower than the duration of the process. When the wave complex reflects from the edge of the target

(curves e,f) another maximum of damage arises in the vicinity of the edge, which has a higher value than the maximum at the impact site.

The volumetric damage parameter ω development is shown on the Fig. 6.11. It is seen that it begins to rise only when the state of the material changes to decompression; in our case it starts when the wave complex reflects from the edge of the target (curves e,f). The damages grow then rather quickly (for the set of parameters used in calculations), and the maximum of the parameter ω is near the edge of the target at the distance equal to the size of the projectile.

The Fig. 6.12 shows the development of the specific dissipation energy D. Its picture is very close to the picture of the shear damage α development; the only difference is that the dissipation almost does not rise at the impact site after the wave complex has passed it by (curves c-f) and that the growth of dissipation in the vicinity of the target's edge is higher due to both damage parameters α and ω contribution to the energy dissipation.

The Fig. 6.13 show the development of the velocity at the edge of the target opposite to the impact site versus time. It is seen that the velocity rises up to $\approx$600m/s$<V_0$=800m/s, then stays for about 1μs decreasing slightly and then falls to $\approx$95m/s. Afterwards it increases gradually up to 120m/s until we stop following it.

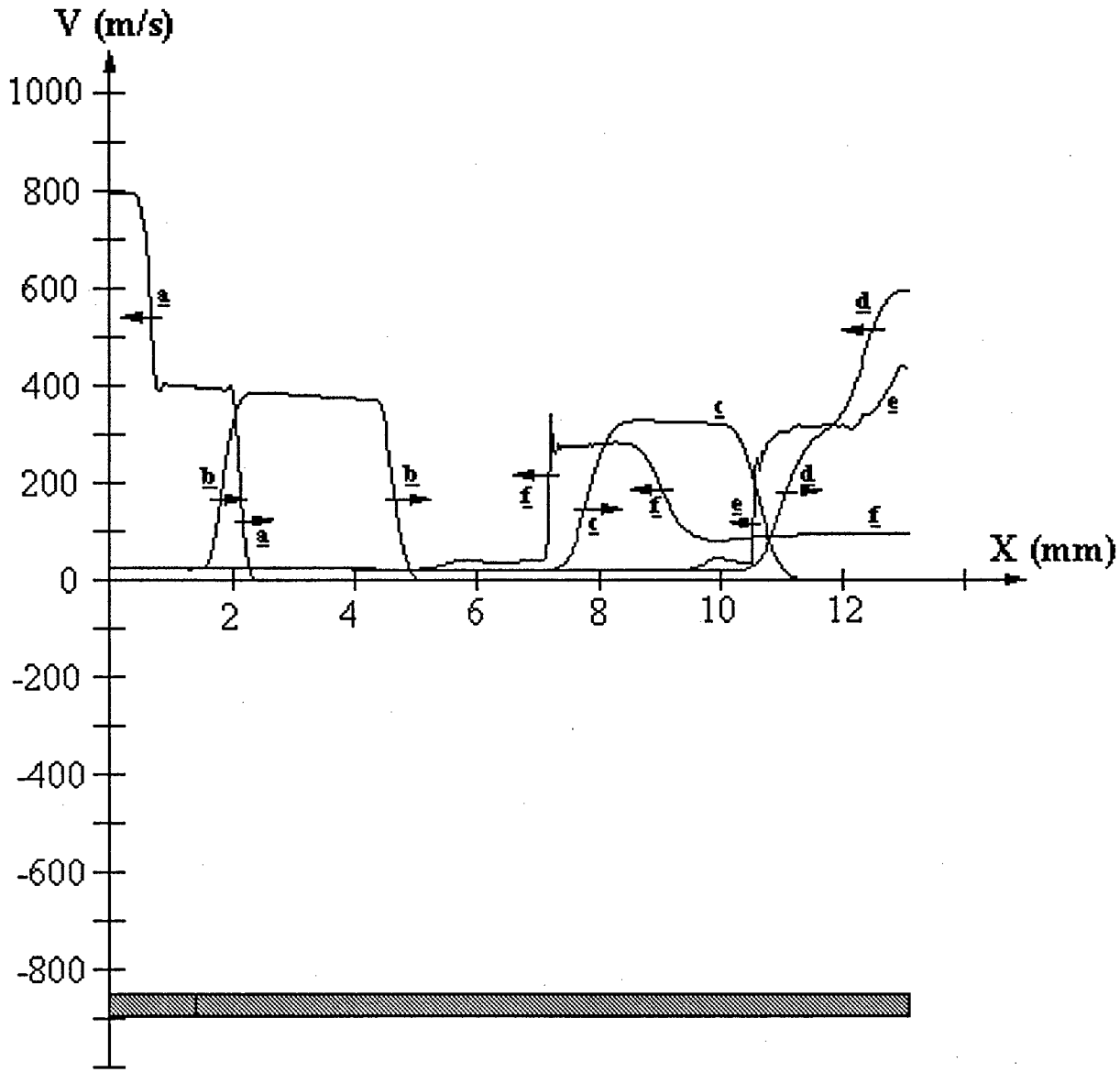

Fig.6.6.

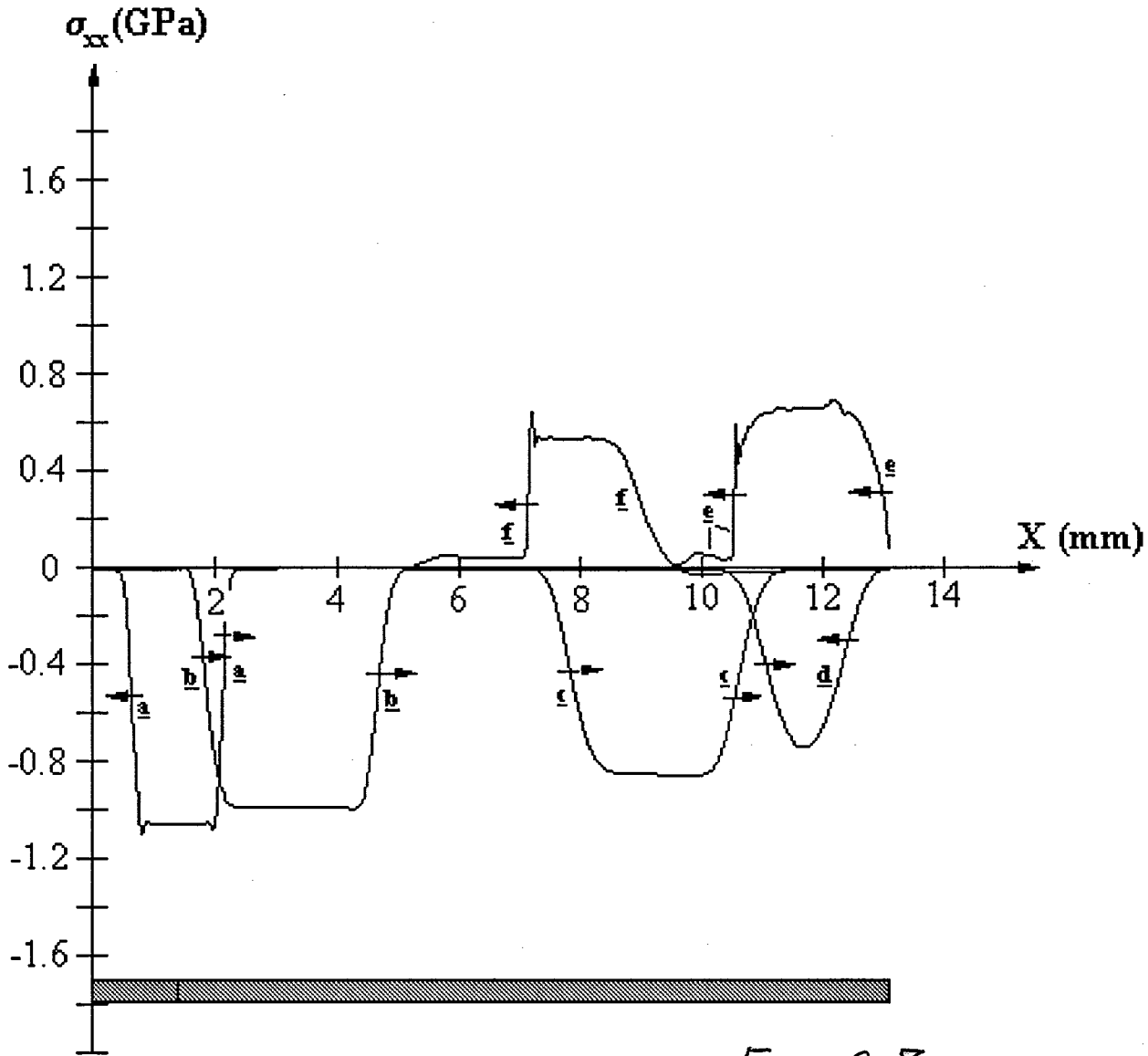

Fig. 6.7.

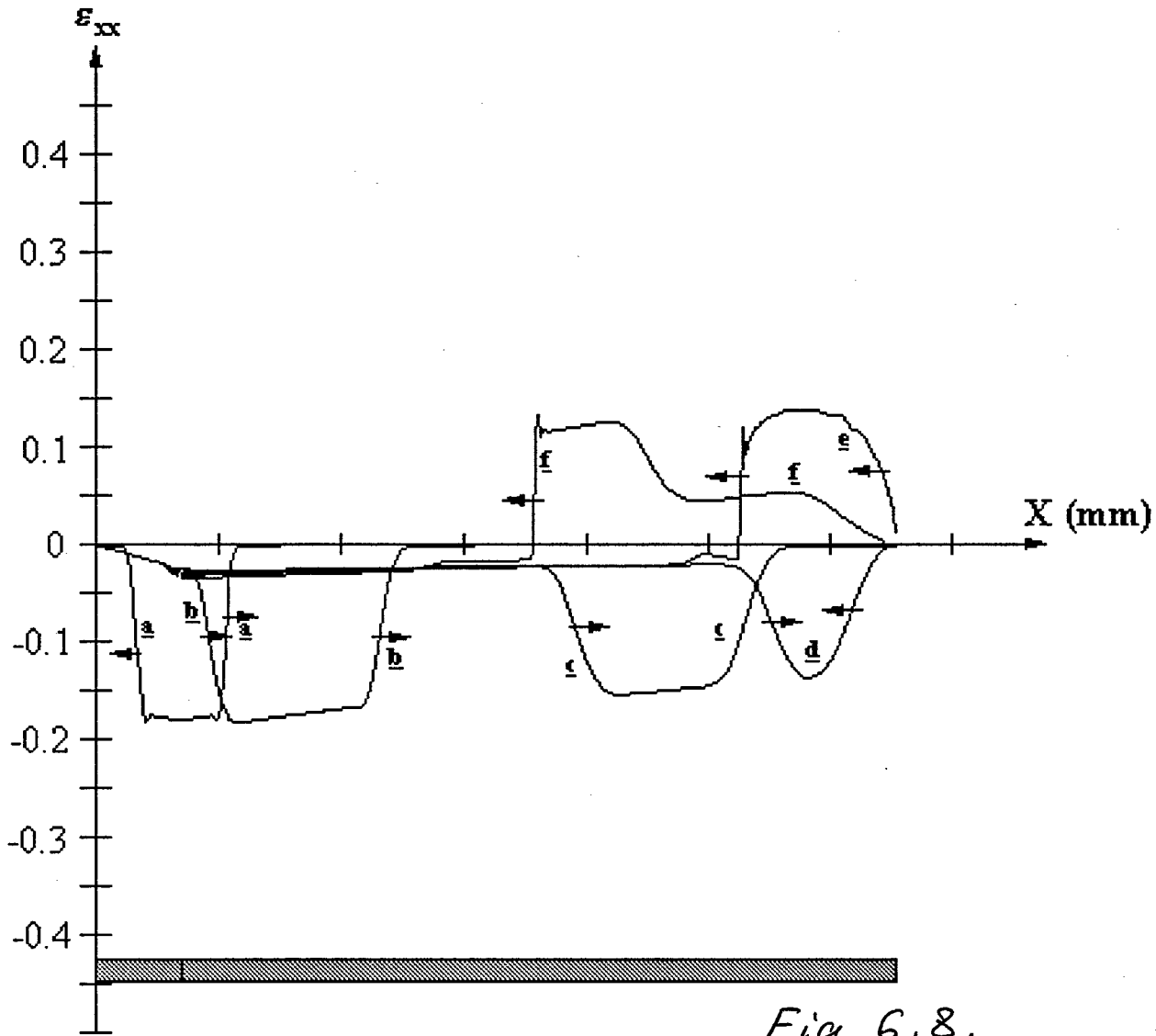

Fig. 6.8.

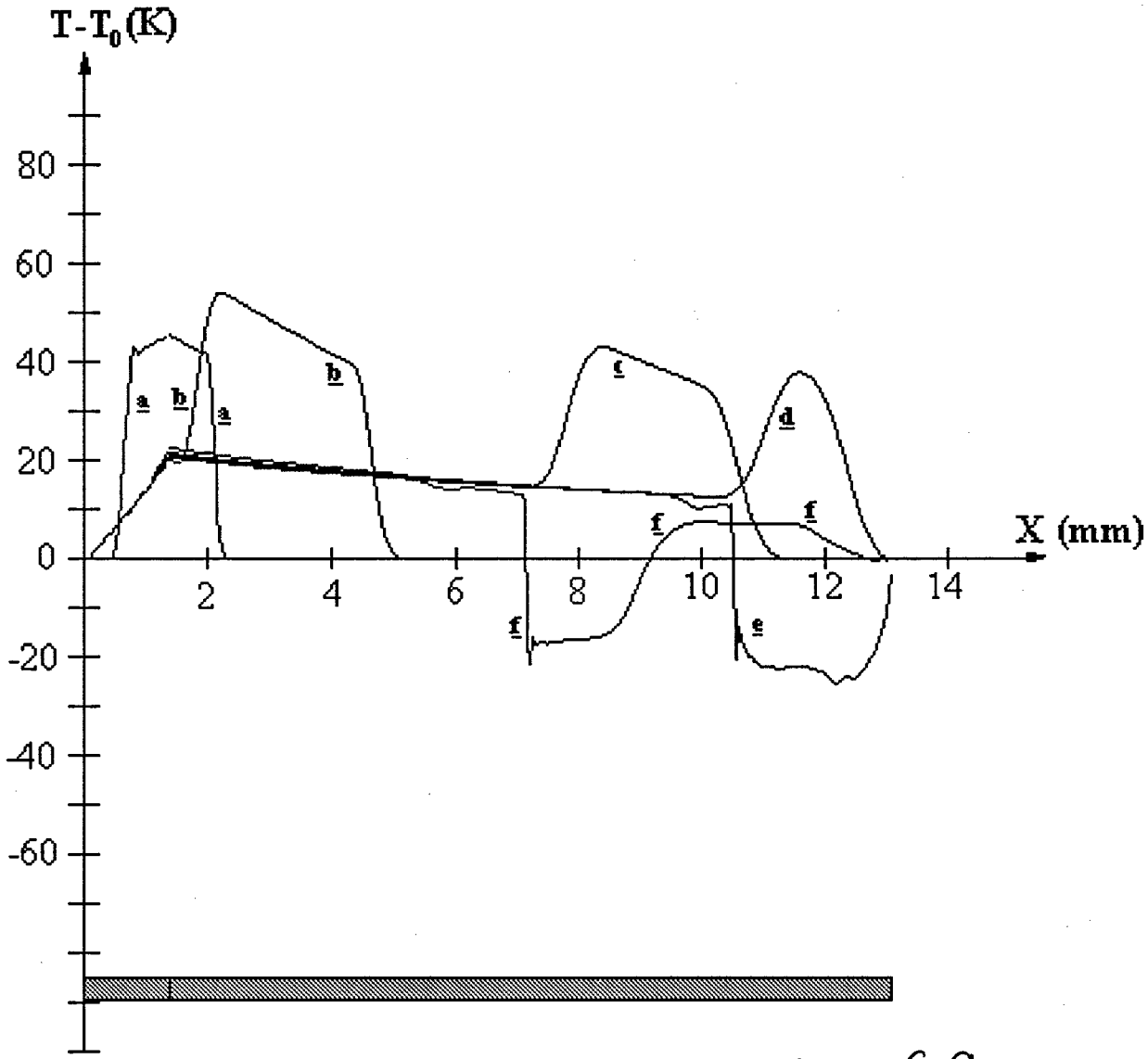

Fig. 6.9.

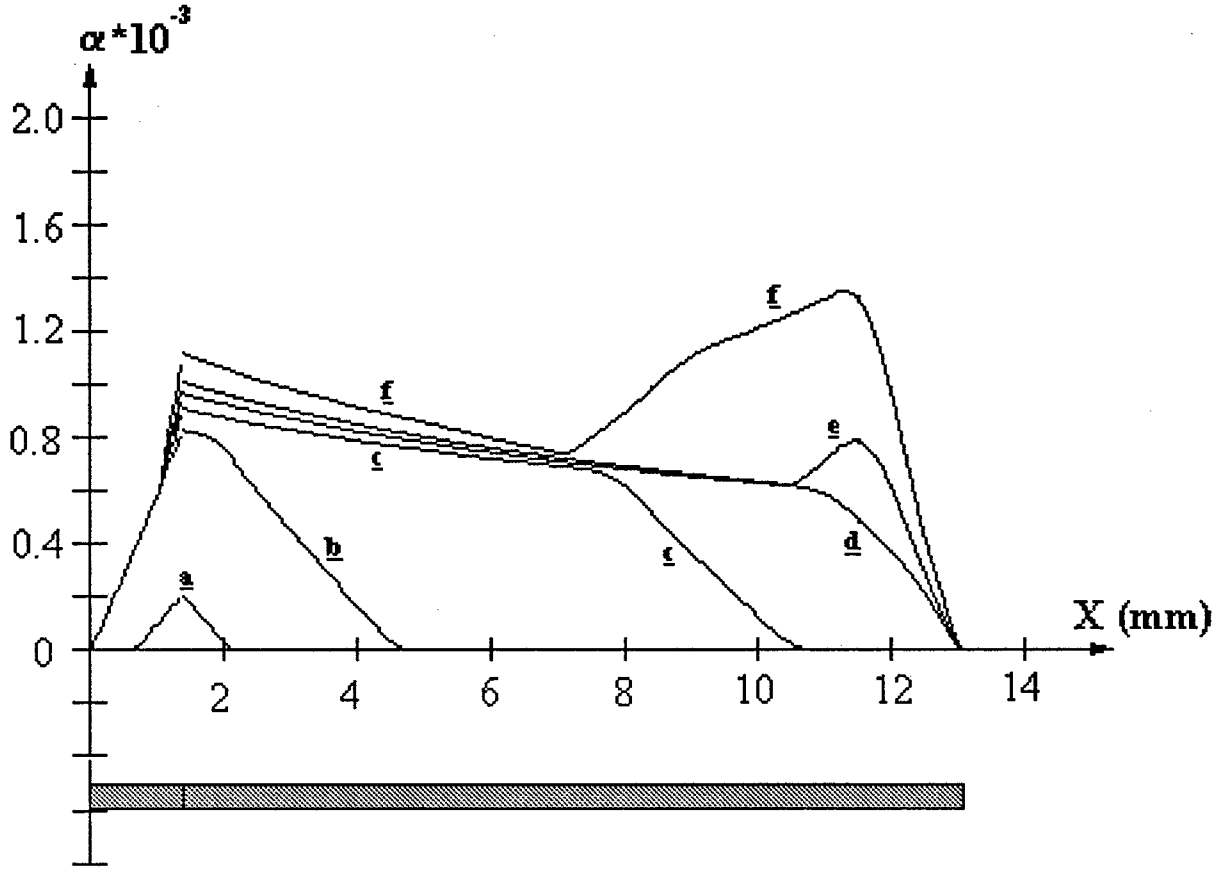

Fig. 6.10.

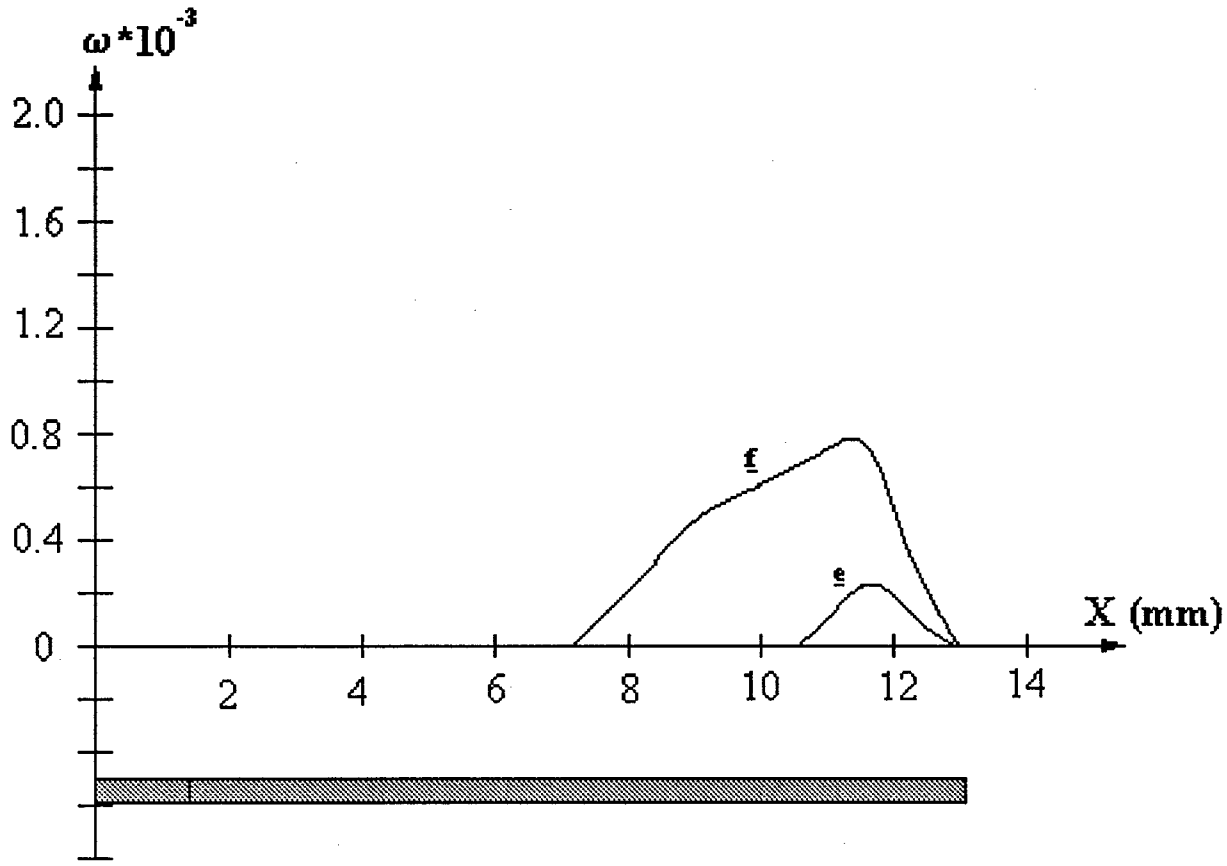

Fig. 6.11.

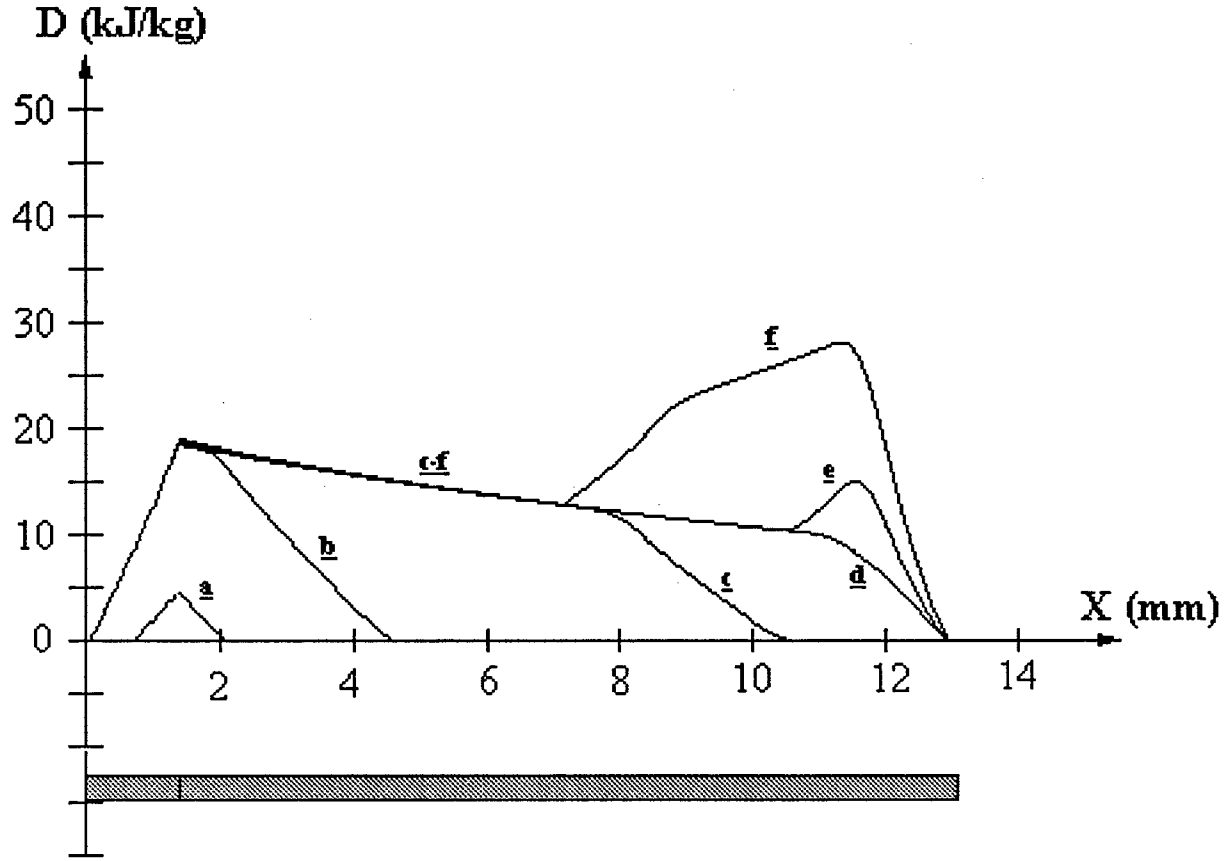

Fig. 6.12.

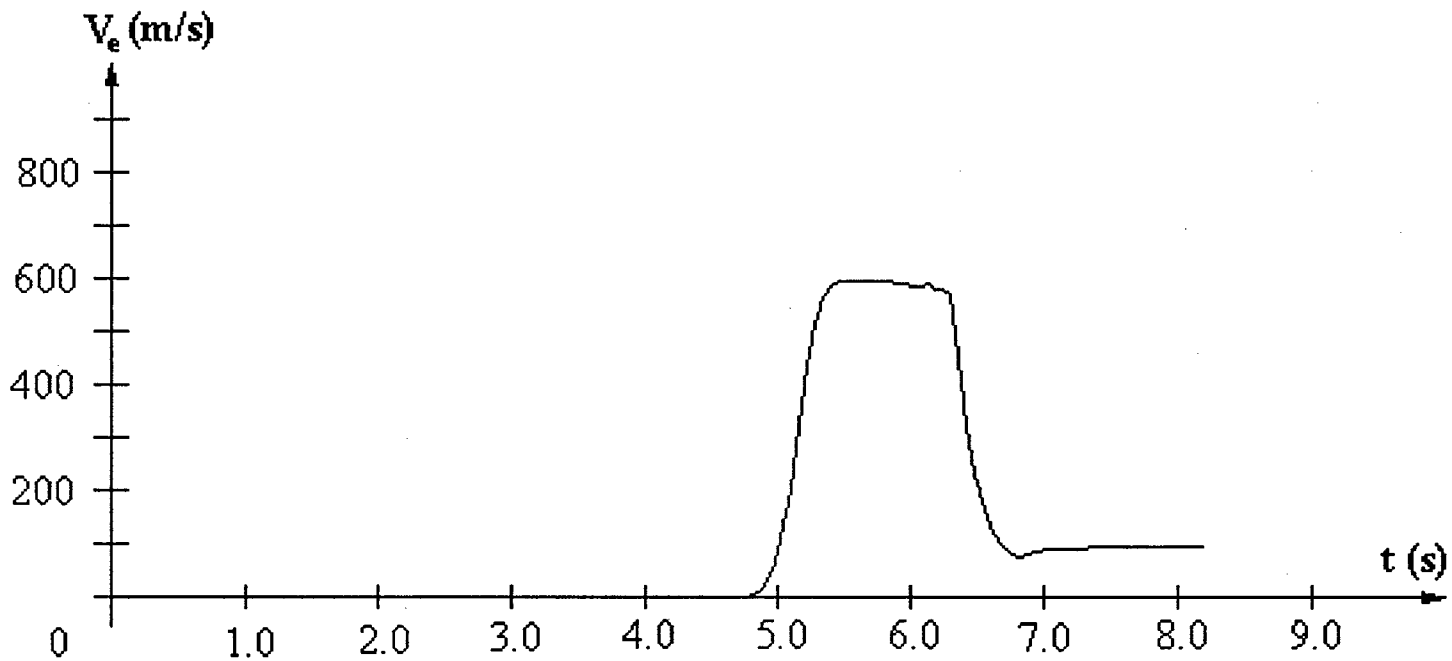

Fig. 6.13.

6.3 Comparison with the experiment and estimations of the damage parameters

The two sets of calculations for visco-elastic and damageable cases illustrated in the previous section show the difference of the material behavior in both cases and also give us some considerations for the different parameters influencing various elements of the experimental curve. In this section we will try to get some estimations of the damage parameters of the plexiglass that could be processed from the experimental data available in [6].

The experimentally measured surface velocity variations of the plexiglass target are shown on the Fig. 6.14. It is seen that velocity reaches its maximum in reflection of the primary compression wave (V_m). Then it comes to a minimum (V_n) in reflection of the decompressive wave, starts growing up again, but the growth is terminated and higher frequency oscillations of the velocity with smaller amplitudes indicate the formation of the spallation plate and multiple reflections of the waves from both free surfaces of the spallation plate. Thus the time of the breakup can be easily detected from the diagram 6.14.

6.3.1 The shear damage factors

One of the main conclusions from the previous results is that the maximum of the target's free surface velocity V_m is independent of the damage parameters governing the volumetric damage ω behavior because the last is not zero only after the leading wave is reflected from the edge of the target. However, V_m is an essential function of the damage parameters governing the shear damage α because of the difference of its value in the visco-elastic and the damageable cases.

The following term from the expression for stress σ_{xx}:

$$AC(1-\omega)^{-1}\log(1-\alpha)\mathrm{sign}(\varepsilon_{xx})$$

is the main term governing difference of the dynamics of the damageable material behavior from that for the visco-elastic case at the first the stage of the process. The first stage of the process is the one when the material is compressed and the wave complex moves towards the right edge of the target. One can see that here $1-\omega = 1$ and the value of $\log(1-\alpha)$ is almost proportional to the kinetic factor C when $\alpha \ll 1$ and the shear deformation exceeds the limit several times. So we can prove and then illustrate the hypothesis: $V_m = V_m(AC^2)$. Of course it is also the function of C independently on AC^2 (due to non-linearity), but most of all the maximal velocity depends on this complex: $\Phi_\alpha = AC^2$.

To illustrate this, the dependence of V_m on Φ_α was build for different values of C (Fig. 6.15). The values of Λ and Ω were varied in the intervals $10^3 \div 10^9$ and $10^3 \div 2 \cdot 10^6$ correspondingly. The experimental value of V_m is 620m/s [6].

It is seen that the diagram of V_m versus Φ_α is practically independent on both C (varied from 10^3 to 10^6) and the volumetric damage parameters Ω and Λ. The curves for

different kinetic factors C are close to each other, and the independence of V_m on Λ and Ω is observed. The coarse logarithmic scale of the Φ_α axis on the Fig. 6.15 helps us to estimate the order of $\Phi_\alpha \approx 10^{15}$Pa/s which gives a coincidence with the experiment.

The Fig. 6.16 shows the dependence of V_m on Φ_α and C in the vicinity of the intersection with the experimental value of V_m. It is seen that at $C = 10^3 s^{-1}$ the best value of Φ_α is $1.08 \cdot 10^{15}$Pa/s, and for $C = 10^6 s^{-1}$ the best value is $\Phi_\alpha = 1.02 \cdot 10^{15}$Pa/s. A small difference between two values (plus the possible experimental error of $5 \div 10\%$) brings to the conclusion that the value of Φ_α can be located well enough for a big variety of C values, and could be taken as about $\Phi_\alpha = 1.05 \cdot 10^{15}$Pa/s for plexiglass. The kinetic factor C independently from Φ_α has a poor influence on the resulting V_m and can not be located separately.

6.3.2 The volumetric damage factors

The experimental curve of the velocity versus time has another critical point: V_n, which is the minimal velocity of the target's edge after the wave complex reflects from it. It is also seen well enough on the calculated curve at the Fig. 6.13. We introduce the hypothesis: for the given value of Φ_α, the value of V_n depends mainly on the following complex of the volumetric damage parameters:

$$\Phi_\omega = \Lambda \Omega^2.$$

It can also depend slightly on C and Ω.

The Fig. 6.17 illustrates the dependence of V_n on Φ_ω for different values of C and Ω. The value of Φ_α was chosen in accordance with the value of C in order to maintain V_m=620m/s (with a help of the data obtained previously and illustrated on the Fig. 6.16).

The curves on the Fig. 6.17 are passing close to the experimental level of V_n=480m/s but could not be extended further to the right because of the premature breakup of the target before the velocity on the target's edge reaches its minimum. This breakup in calculations can be delayed a little if we increase the level of D_* up to $3 \cdot 10^6$J/kg but the dissipation is rising up at the breakup site very rapidly.

It can be seen from the Fig. 6.17 that the dependencies of V_n on Φ_ω are close to each other for different values of C and Ω. The intersection with the experimental level V_n=480m/s is approximately at $\Phi_\omega = 3 \cdot 10^{16}$ Pa/s. So the results show that the complex of the volumetric damage parameters Φ_ω is an order of magnitude higher than the complex Φ_α for the shear damage parameters. Thus the dissipation growth rate due to volumetric damage is an order of magnitude higher (for plexiglass, in particular) than that due to shear damage.

The Fig. 6.18 illustrates the details of V_n dependence on C and Ω with more fine scales than in the Fig. 6.17 and closer to the interval we are interested in. It is seen that V_n is practically independent of Ω and there is a slight dependence on C (about 2%). The results show that the value of Φ_ω must be within the interval of $3.0 \div 3.2 \cdot 10^{16}$Pa/s.

The result $\Phi_\omega = 3.0 \cdot 10^{16}$Pa/s gives us a very important estimate for the volumetric damage parameters set.

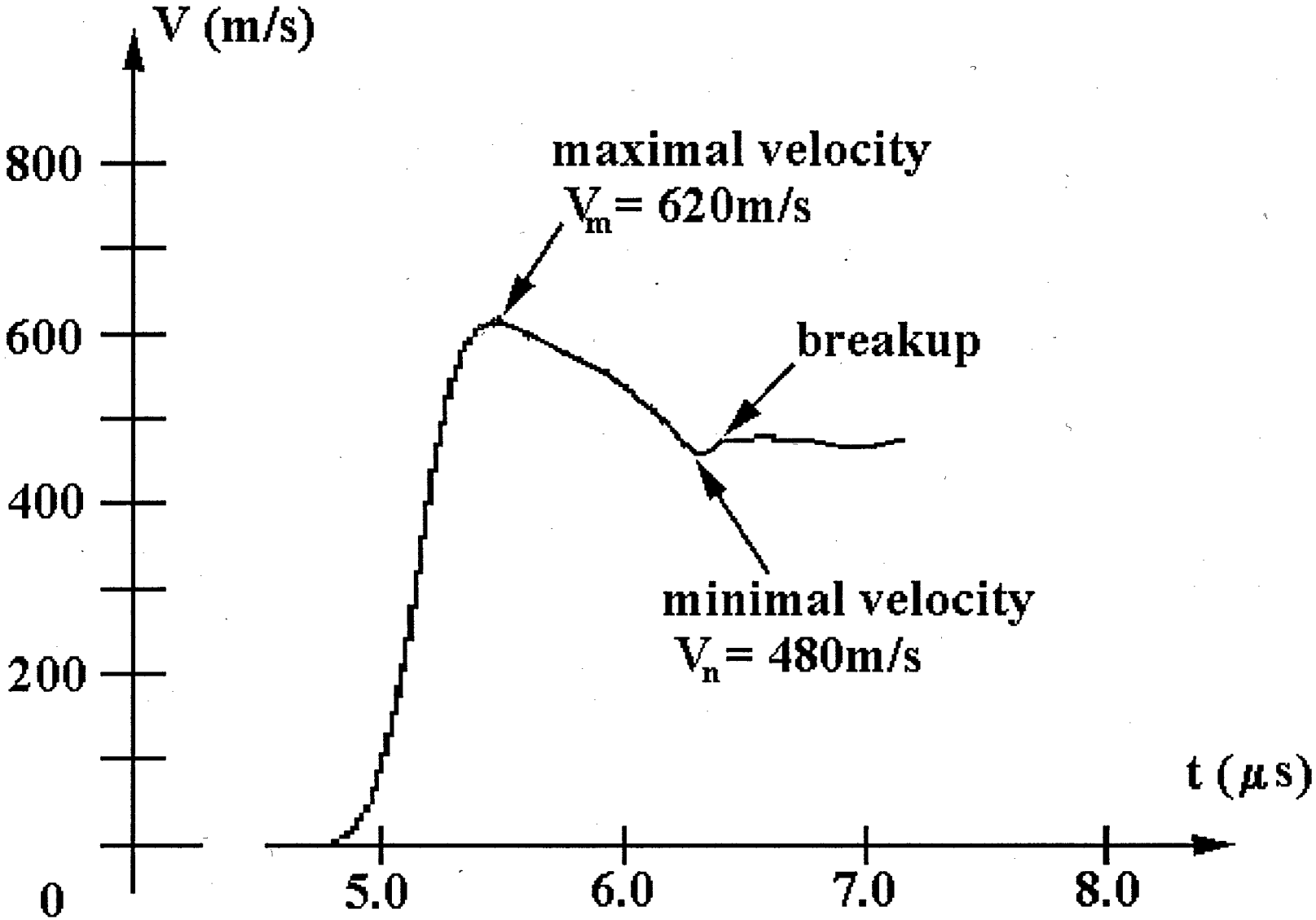
V (m/s)
800
600
400
200
0
maximal velocity
V_m = 620m/s
breakup
minimal velocity
V_n = 480m/s
t (μs)
5.0
6.0
7.0
8.0

Fig. 6.14.

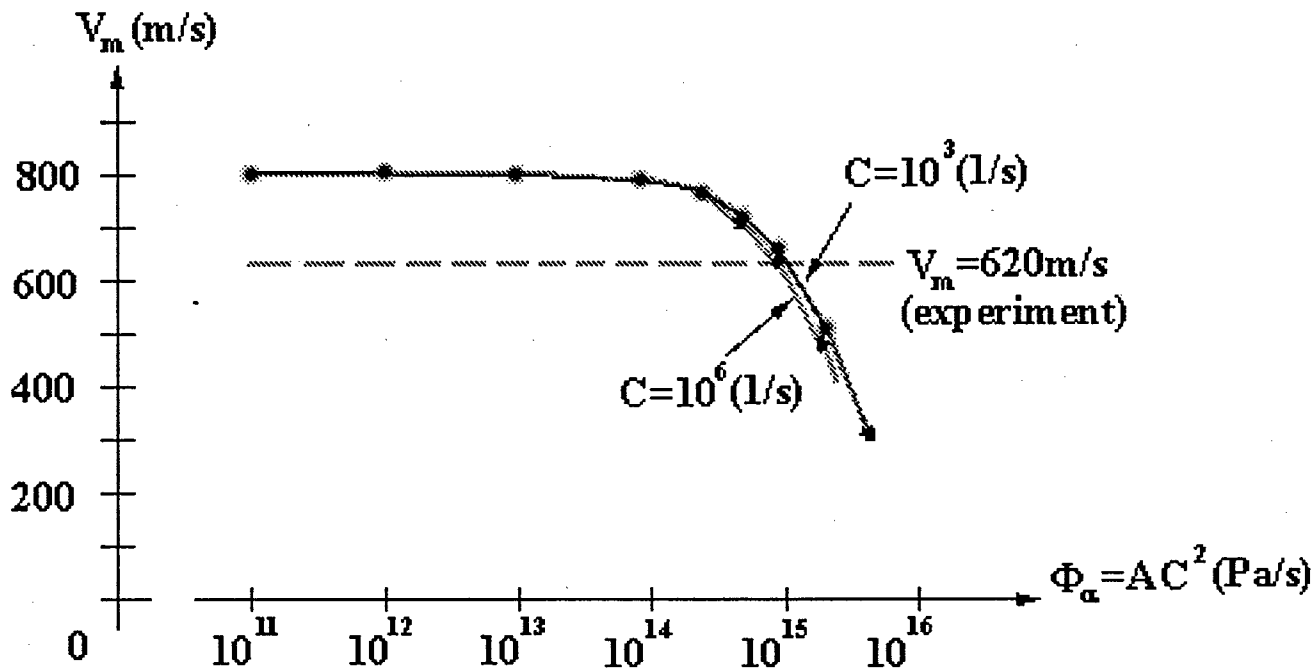
V_m (m/s)
800
600
400
200
0
10^{11}
10^{12}
10^{13}
10^{14}
10^{15}
10^{16}
$\Phi_\alpha = AC^2$ (Pa/s)
$C=10^3$ (1/s)
V_m=620m/s
(experiment)
$C=10^6$ (1/s)

Fig. 6.15

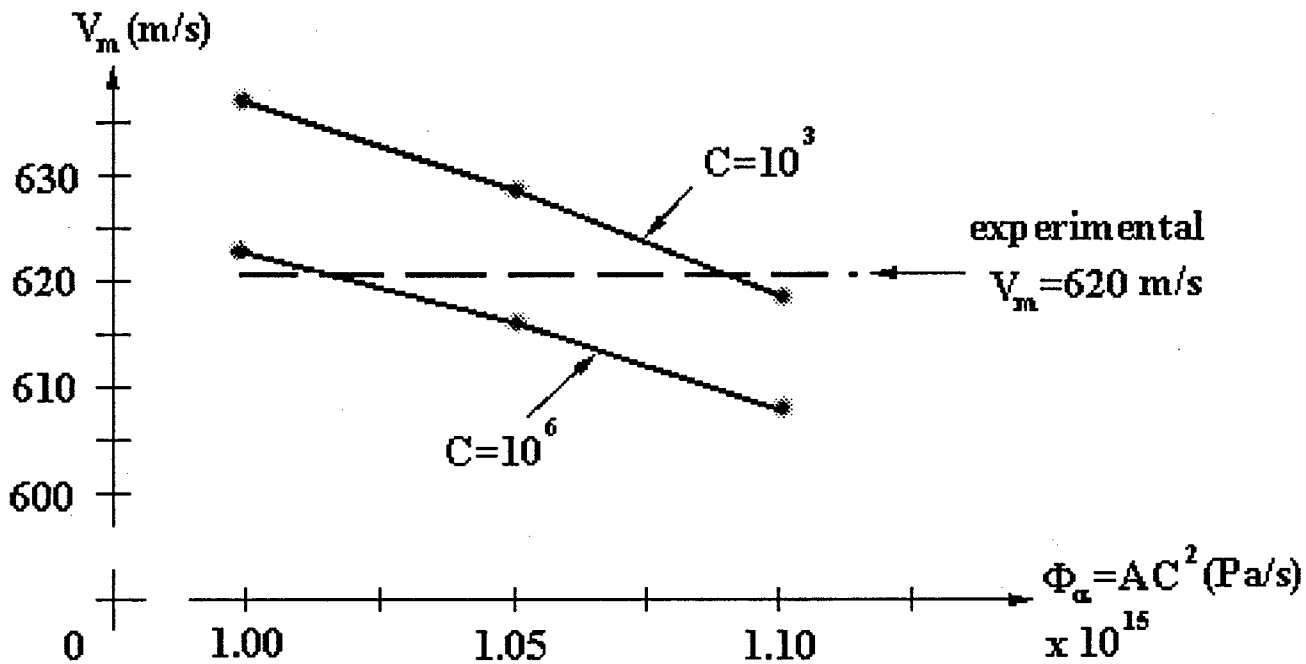
V_m (m/s)
630
620
610
600
0
1.00
1.05
1.10
$C=10^3$
$C=10^6$
experimental
V_m=620 m/s
$\Phi_\alpha=AC^2$(Pa/s)
x 10^{15}

Fig. 6.16.

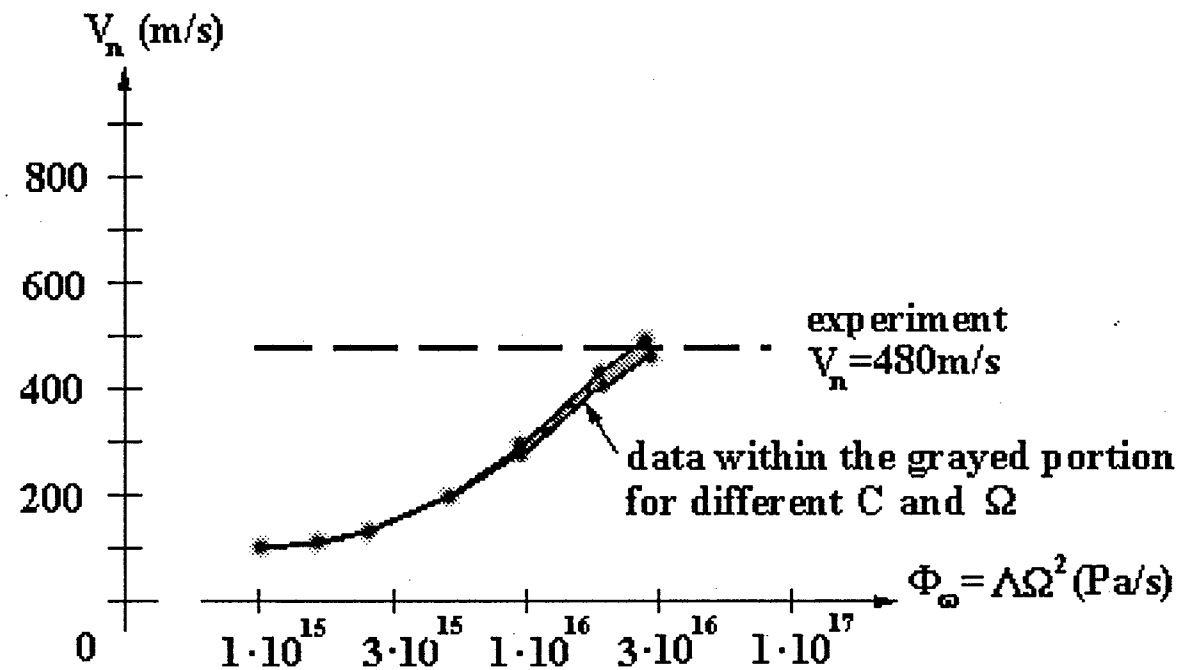
V_n (m/s)
800
600
400
200
0
experiment
V_n=480m/s
data within the grayed portion
for different C and Ω
$\Phi_\omega = A\Omega^2$ (Pa/s)
$1 \cdot 10^{15}$
$3 \cdot 10^{15}$
$1 \cdot 10^{16}$
$3 \cdot 10^{16}$
$1 \cdot 10^{17}$

Fig. 6.17.

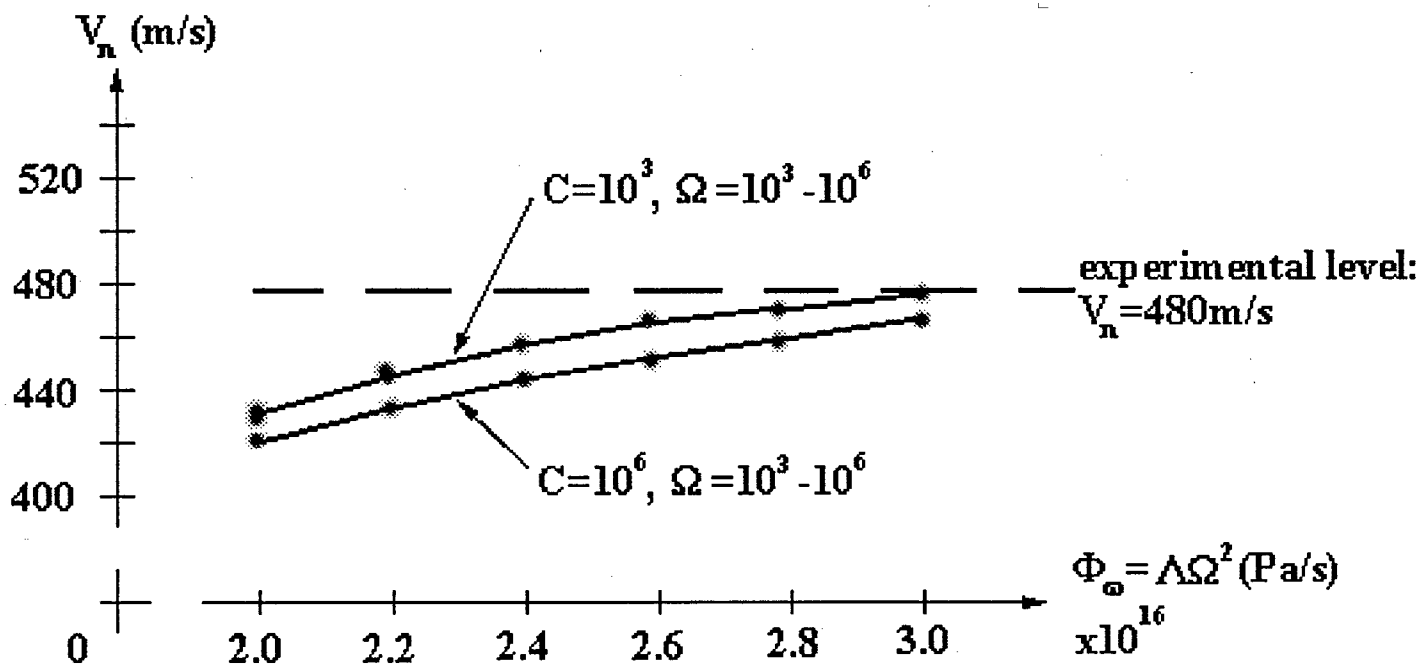
V_n (m/s)
520
480
440
400
0
2.0
2.2
2.4
2.6
2.8
3.0
$C=10^3$, $\Omega=10^3$ -10^6
$C=10^6$, $\Omega=10^3$ -10^6
experimental level:
V_n=480m/s
$\Phi_\omega=\Lambda\Omega^2$ (Pa/s)
x10^{16}

Fig. 6.18

6.3.3 Comparison with the shape of the experimental curve. Considerations about the values of kinetic parameters and the critical dissipation

The previous sections 6.2.1 and 6.2.2 where the complexes $\Phi_\alpha = AC^2$ and $\Phi_\omega = \Lambda\Omega^2$ were estimated using the two main features of the experimental curve – velocities V_m and V_n – gave us a little information about the actual values of C, Ω and D_*.

Here we give some considerations about the values of damage kinetic factors Ω and C comparing the shape of the experimental curve with shapes of the curves obtained by calculations with different values of Ω and C. The enthropy factors Λ and A for those calculations are obtained using the estimations of Φ_ω and Φ_α:

$$\Lambda = \frac{\Phi_\omega}{\Omega^2}, \qquad A = \frac{\Phi_\alpha}{C^2}.$$

The value of Φ_α was chosen within the interval $[1.02 \cdot 10^{15}, 1.10 \cdot 10^{15}]$ for different C in order to maintain $V_m = 620\text{m/s}$ (using the diagram in the Fig. 6.16). The value of Φ_ω was taken as $3.0 \cdot 10^{16}$.

The Fig. 6.19 illustrates the calculated curves of the target's edge velocity $V(t)$ versus time. The breakup moment is marked with a cross on each curve. The experimental curve [6] is also shown. Each calculated curve is marked with the set of values Ω and C used in calculations; the other damage parameters are maintained as described above. The time scale on the Fig. 6.19 has the origin at the initial impact.

It is seen from the Fig. 6.19 that the shape of the calculated curves is practically independent of the volumetric kinetic factor Ω. However the shear kinetic factor C has an influence: the higher C the closer it passes to the experimental curve. However the difference remain sufficient at $C = 1.4 \cdot 10^6$. But our attempts to rise the value of C higher brought to premature breakup at the impact site which was not recorded in the experiment [6].

As it is seen from the Fig. 6.19, the order of magnitude of the kinetic factors is determined nevertheless: the sufficient change in the shape of the calculated curves begins with $C = 1.0 \cdot 10^6(1/\text{s})$; and the curve at $C = 1.4 \cdot 10^6$ is passing much closer to the experimental curve than at $C = 10^6$.

The experimental data enables us to determine the time for the spallation plate separation. That means that by that time the dissipation function in the zone of spallation formation reaches the critical value D_*.

In order to examine the possible estimation of the specific dissipation critical level D_* we processed a series of calculations with the damage parameters which give the closest possible coincidence with the experiment [6]: $\Phi_\alpha = 1.00{\cdot}10^{15}$, $C = 1.4{\cdot}10^6$, $\Phi_\omega = 3.00{\cdot}10^{16}$, $\Omega = 10^6$. The value of the volumetric kinetic factor Ω was taken using a consideration that it must be of the same order as the correspondent shear factor. Each time in this series we checked up the breakup moment and examined the location of the breakup site, the fact whether the velocity at the edge of the target had passed its minimum before

the breakup and the final velocity which must not differ essentially from the final velocity obtained in the experiments.

The results are shown in the Table 6.4. Here D_* is the assumed critical dissipation level and V_f is the final velocity of the target obtained after the breakup.

D_*, J/kg	V_f, m/s	Notes on the breakup
$1.0 \cdot 10^4$	0	premature breakup at the impact site
$1.0 \cdot 10^5$	577	before the velocity reaches minimum
$3.0 \cdot 10^5$	483	before the velocity reaches minimum
$1.0 \cdot 10^6$	459	before the velocity reaches minimum
$1.1 \cdot 10^6$	457	very close to the velocity minimum
$1.2 \cdot 10^6$	460	soon after the velocity reached its minimum
$2.0 \cdot 10^6$	460	soon after the velocity reached its minimum

Table 6.4. Different values of D_* level affect the conditions at the breakup.

It is seen from the Table 6.4 that the most acceptable value of D_* is about $1.1 \div 1.2 \cdot 10^6$J/kg. On one hand, the velocity of the target's edge had really reached and passed its minimum in the experiment [6]. On the other hand, further increase of the critical dissipation level contributes nothing more to the final state after the breakup. In fact, the calculations on the model had shown that after the dissipation D reached some level of the order of 10^6J/kg anywhere within the material, its irreversable growth changed to be extremely rapid. In those circumstances any further increase of the critical level D_* does not change essentially the time moment of the breakup.

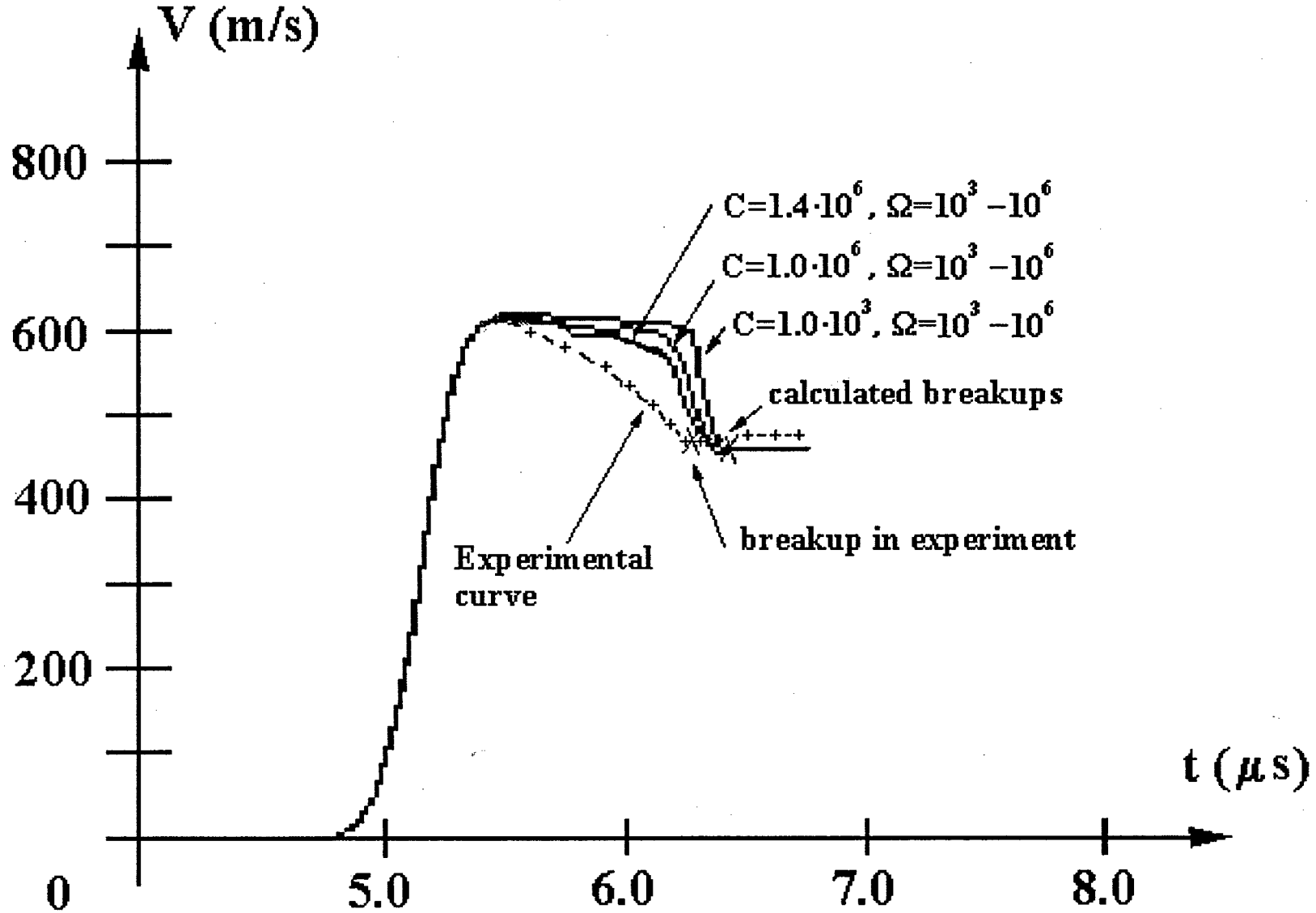
V (m/s)
800
600
400
200
0
5.0
6.0
7.0
8.0
t (μs)
C=1.4·10^6, Ω=10^3 –10^6
C=1.0·10^6, Ω=10^3 –10^6
C=1.0·10^3, Ω=10^3 –10^6
calculated breakups
Experimental curve
breakup in experiment

Fig. 6. 19.

Conclusions to chapter 6

- The detailed investigation of two plexiglass samples high-velociy collision was processed using the pure visco-elastic model and the model with the damages growth. The difference of results for two models was illustrated together with the influence of different constants regulating the damages evolution (damage parameters) on the behavior of the material.

- It was obtained that in case of high-velocity impact when the deformations in the sample exceed the elasticity limit several times, the maximum of the velocity on the edge of the target sample V_m depends mainly on the complex made of the shear damage parameters $\Phi_\alpha = AC^2$ where A is the shear enthropy factor and C is the shear kinetic factor.

- When the stress waves reflect from the target's edge, its velocity decreases to zero in the non-damageable case and to $V_n > 0$ in the damageable one. It was obtained that the value of V_n depends mainly on the complex combined of the volumetric damage parameters: $\Phi_\omega = \Lambda\Omega^2$, where Λ is the volumetric enthropy factor and Ω is the volumetric kinetic factor.

- Comparison with the experiment on the plexiglass samples high-velocity collision helped to obtain the estimations $\Phi_\omega \approx 1.0 \cdot 10^{15}$Pa/s and $\Phi_\alpha \approx 3.0 \cdot 10^{16}$Pa/s using the experimental values of V_m and V_n respectively. The comparison of the shapes of the calculated curves to the shape of the experimental one helped to estimate the order of the shear damage kinetic factor $C \approx 1.4 \cdot 10^6$. The estimate for the volumetric kinetic factor was not obtained because the calculations had shown the independence of the shape of the experimental curve on this factor. Finally, the critical level of the specific dissipation D_* was estimated to be $\approx 1.2 \cdot 10^6$J/kg in order to ensure the absence of the premature breakup (either at the impact site or before the velocity on the target's edge reaches its minimal value V_n).

References

1. Smirnov N.N., Kiselev A.B., Nikitin V.F., Shevtsova V.M. and Yumashev M.V. First Interim Report on SPC 97-4046. – Moscow-Brussels, 1997, 38 p.

2. Smirnov N.N., Kiselev A.B., Nikitin V.F., Shevtsova V.M. and Yumashev M.V. Second Interim Report on SPC 97-4046. – Moscow-Brussels, 1997, 35 p.

3. Smirnov N.N., Kiselev A.B., Nikitin V.F., Shevtsova V.M. and Yumashev M.V. Final Report on SPC 97-4046. – Moscow-Brussels, 1998.

4. Smirnov N.N., Kiselev A.B., Nikitin V.F., Shevtsova V.M. and Yumashev M.V. First Interim Report on SPC 98-4070. – Moscow-Brussels, 1998.

5. Smirnov N.N., Kiselev A.B., Nikitin V.F., Shevtsova V.M. and Yumashev M.V. Second Interim Report on SPC 98-4070. – Moscow-Brussels, 1999.

6. Parkhomenko I.P., Utkin A.V., Separation durability of the plexiglass. In: "Investigation of materials properties at extreme conditions" edited by Fortov V.E., Kudrenkov E.A. – Moscow, Computing Technology Institute of Russian Academy of Sciences, 1990.

Conclusions

The results of investigations show that the damage parameters for the laminated thermo-viscoelastic composite materials could be developed based on the results of two types of experiments: low and high rates of loading.

The experiments on high rates of loading (impact experiments; Chapters 5 and 6) make it possible to evaluate: the tension and shear damage enthropy factors (Λ and A), the shear damage kinetic factor (C) and the critical breakup dissipation D_* with a sufficient accuracy. While the magnitudes of the critical deformations ε_*, ε_τ^*, ε_Δ^*, which regulate the accumulation of damages in tension, shear and delamination respectively, cannot be evaluated in the impact experiments. The reason is that in high-velocity impact experiments the critical values of deformations are exceeded several times in compression and decompression waves travelling in the sample.

The experiments on low rates of loading (twisting and stretching of tubular samples, Chapters 3 and 4) make it possible to evaluate the rest of parameters: critical deformations ε_*, ε_τ^* and ε_Δ^*, volumetric and delamination damage kinetic factors Ω and Ω_Δ, delamination damages enthropy factor Λ_Δ, – with a sufficient accuracy, while the breakup criterion – the critical dissipation D_* – cannot be developed from low velocity loading experiments with a necessary accuracy.

Thus the combination of the two developed methodologies: the ones for low and high velocity loadings makes it possible to develop all the 10 damage parameters for composite materials.

Processing the experimental results on organic glass high-velocity impact enabled to develop the critical dissipation D_* (the breakup criterion) and the three other damage parameters (volumetric enthropy and shear enthropy and kinetic factors).

Analysis of the developed methodology and the first results show that the damage parameters could be determined for all the types of two-phase laminates in experiments conducted for each type of materials; while the other material constants (shear modulus, volumetric elastic modulus, specific heat capacity, etc.) could be determined for each phase independently and then recalculated to obtain the value for a two-phase laminate.

The main target of the future research on improving the computational damage model for the laminated composite materals would be the construction of a model enabling to develop the damage parameters for all the types of two-phase composite materials based on independent experiments with its phases. Then the damage parameters for two-phase material should be introduced as functions of the phases concentration and phases properties for the laminate. Such an improvement of the model will make it possible to

determine once the damage characteristics for phases of the laminate, and then to evaluate the damage parameters for different types of laminates composed of those phases.